Published for SISSA by Springer

Received: *August 28, 2023*
Revised: *November 5, 2023*
Accepted: *January 23, 2024*
Published: *February 13, 2024*

Measurement of the Z boson production cross-section in pp collisions at $\sqrt{s} = 5.02$ TeV

The LHCb collaboration

E-mail: yuhaow@cern.ch

Abstract: The first measurement of the Z boson production cross-section at centre-of-mass energy $\sqrt{s} = 5.02\,\text{TeV}$ in the forward region is reported, using pp collision data collected by the LHCb experiment in year 2017, corresponding to an integrated luminosity of $100 \pm 2\,\text{pb}^{-1}$. The production cross-section is measured for final-state muons in the pseudorapidity range $2.0 < \eta < 4.5$ with transverse momentum $p_{\mathrm{T}} > 20\,\text{GeV}/c$. The integrated cross-section is determined to be

$$\sigma_{Z\to\mu^+\mu^-} = 39.6 \pm 0.7(\text{stat}) \pm 0.6(\text{syst}) \pm 0.8(\text{lumi})\,\text{pb}$$

for the di-muon invariant mass in the range $60 < M_{\mu\mu} < 120\,\text{GeV}/c^2$. This result and the differential cross-section results are in good agreement with theoretical predictions at next-to-next-to-leading order in the strong coupling constant.

Based on a previous LHCb measurement of the Z boson production cross-section in pPb collisions at $\sqrt{s_{\mathrm{NN}}} = 5.02\,\text{TeV}$, the nuclear modification factor $R_{p\mathrm{Pb}}$ is measured for the first time at this energy. The measured values are $1.2^{+0.5}_{-0.3}(\text{stat}) \pm 0.1(\text{syst})$ in the forward region ($1.53 < y^*_\mu < 4.03$) and $3.6^{+1.6}_{-0.9}(\text{stat}) \pm 0.2(\text{syst})$ in the backward region ($-4.97 < y^*_\mu < -2.47$), where y^*_μ represents the muon rapidity in the centre-of-mass frame.

Keywords: Electroweak Interaction, Hadron-Hadron Scattering , QCD

ArXiv ePrint: 2308.12940

https://doi.org/10.1007/JHEP02(2024)070

JHEP02(2024)070

Contents

1 Introduction

The $pp \to Z \to \mu^+\mu^-$ process[1] is highly interesting for probing the quantum chromodynamics (QCD) and electroweak (EW) sectors. Particularly, precision measurements of the Z boson production cross-section at various experiments offer valuable insights for testing Standard

[1] The production process should be interpreted as $pp \to Z/\gamma^* \to \mu^+\mu^-$ in the strict sense. In this article, the label Z boson is defined to also include contributions from virtual photons and the interference between the Z boson and the virtual photon.

Model predictions [1–9], which are obtained from precision perturbative QCD calculations up to the order of α_s^3 [8, 9].

High precision measurements of the Z boson production cross-sections at different rapidities at LHCb have imposed important constraints on parton distribution functions (PDFs). Results from deep inelastic scattering and hadronic collisions [10–25], parameterized in terms of the Bjorken variable, x, indicating the fraction of the proton momentum carried by a single parton, are used in the global fits of the PDFs. However, these measurements provide limited information on the PDFs in the very large ($x \sim 0.8$) or very small ($x \sim 10^{-4}$) Bjorken-x regions. This leads to large uncertainties on the PDFs, and on the theoretical predictions that make use of them. Forward acceptance of the LHCb detector covers a unique region of phase space, allowing measurements of highly boosted Z boson candidates to be made. Measurements within this region are sensitive to both large and small Bjorken-x values. Previous measurements of single W and Z production by the LHCb collaboration [26–32] have been included in PDF determinations [33–41] and significantly contributed to the precision of the quark PDFs at large and small values of x.

In addition, the Z boson production cross-section is useful for constraining nuclear PDFs (nPDFs), providing a clean probe of nuclear-matter effects in the initial state. These effects are typically studied in terms of the nuclear modification factor, $R_{p\mathrm{Pb}}$, defined as the ratio of the yield observed in pPb collisions to that in pp collisions, scaled by the mean number of nucleon-nucleon interactions. This quantity is used to study the modification of particle production in heavy-ion collisions compared to pp collisions. The LHCb experiment published the first inclusive Z production result in pPb collisions at a nucleon-nucleon centre-of-mass energy of $\sqrt{s_{NN}} = 5.02\,\mathrm{TeV}$ [42]. However, no nuclear modification factor has been reported so far for this collision energy due to the absence of a cross-section measurement in pp collisions. With this new measurement of the Z boson production cross-section in pp collisions at $\sqrt{s} = 5.02\,\mathrm{TeV}$, the nuclear modification factors in the forward region and backward regions are reported here for the first time. The forward and backward regions, defined by the muon rapidity y^*_μ in the pPb centre-of-mass frame, are $1.53 < y^*_\mu < 4.03$ and $-4.97 < y^*_\mu < -2.47$, as the pPb collision system experiences an asymmetric distribution of beam energy.

In this article, the integrated and differential Z boson production cross-sections in different kinematic bins are measured at the Born level in QED, using pp collision data collected by the LHCb detector at a centre-of-mass energy of $\sqrt{s} = 5.02\,\mathrm{TeV}$ in 2017, corresponding to an integrated luminosity of $100\,\mathrm{pb}^{-1}$ [43]. The production cross-sections are measured in a fiducial region that closely matches the acceptance of the LHCb detector, following the analysis strategy developed in ref. [32]. The fiducial region is defined by requiring that both muons have a pseudorapidity in the range of $2.0 < \eta < 4.5$ and transverse momentum $p_\mathrm{T} > 20\,\mathrm{GeV}/c$, and that the di-muon invariant mass is in the interval $60 < M_{\mu\mu} < 120\,\mathrm{GeV}/c^2$.

2 Detector and simulation

The LHCb detector [44, 45] is a single-arm forward spectrometer covering the pseudorapidity range $2 < \eta < 5$, designed for the study of hadrons containing b or c quarks. The detector includes a high-precision tracking system consisting of a silicon-strip vertex detector surrounding the pp interaction region [46], a large-area silicon-strip detector (TT) [47], located

JHEP02(2024)070

upstream of a dipole magnet with a bending power of about 4 Tm, and three stations of silicon-strip detectors and straw drift tubes [48] placed downstream of the magnet. The tracking system provides a measurement of the momentum, p, of charged particles with a relative resolution that varies from 0.5 % at low momentum to 1.0 % at 200 GeV/c. The minimum distance of a track to a primary pp collision vertex, the impact parameter, is measured with a resolution of $(15 + 29/p_{\mathrm{T}})$ µm, where p_{T} is the component of the momentum transverse to the beam, in GeV/c. Photons, electrons and hadrons are identified by a calorimeter system consisting of scintillating-pad and preshower detectors, an electromagnetic and a hadronic calorimeter. Muons are identified by a system composed of alternating layers of iron and multiwire proportional chambers [49]. The online event selection is performed by a trigger [50], which consists of a hardware stage, based on information from the calorimeter and muon systems, followed by a software stage, which applies a full event reconstruction.

Simulation is used to model the effects of the detector acceptance and the imposed selection requirements. In the simulation, pp collisions are generated using Pythia [51, 52] with a specific LHCb configuration [53]. Final state radiation (FSR) is generated using Photos [54]. The interactions of the generated particles with the detector, and its response, are implemented using the Geant4 toolkit [55] as described in ref. [56].

In this paper, three generators are used to calculate the theoretical predictions. The ResBos [57] program performs resummation of large logarithms, achieving accuracy up to the next-to-next-to-leading-logarithm level, within the Collins-Soper-Sterman resummation formalism [58–60] and matches to next-to-leading-order (NLO) fixed order calculations. It also provides theoretical predictions for processes involving FSR corrections and event generation. The enhanced QCD prediction is obtained from the simulated $Z \to \mu^+\mu^-$ sample, generated with ResBos [57] using the CT18 PDFs [36] for all measurements. Powheg-BOX [61–64] is an NLO generator, and can be interfaced with Pythia for QCD and EW showering. Although Pythia is a leading-order (LO) generator, it approximates higher order effects in initial and final states via a parton showering algorithm [65]. In this analysis, Powheg-BOX is used to generate $Z \to \mu^+\mu^-$ events, followed by hadronization using Pythia for all measurements. The MCFM package [66], a fixed-order next-to-next-to-leading-order (NNLO) generator, is used here to estimate the Z boson production cross-section as a function of y^Z in the acceptance of the LHCb detector. For these three generators, different PDFs sets NNPDF3.1 [37], NNPDF4.0 [38], MSHT20 [39], and CT18 [36] are employed to provide theoretical predictions.

3 Event selection and background estimation

The muon triggers are responsible for the online event selection. At the hardware trigger stage, a muon candidate with high p_{T} is required. The muon candidate is required to have $p_{\mathrm{T}} > 6$ GeV/c and $p > 8$ GeV/c, along with a good track fit quality in the first software trigger stage. In the second software trigger stage, an additional requirement of $p_{\mathrm{T}} > 12.5$ GeV/c is imposed on the muon candidate. For a $Z \to \mu^+\mu^-$ candidate, it is necessary for at least one of the muons to pass both the hardware and software trigger stages.

A high-purity $Z \to \mu^+\mu^-$ sample is reconstructed from a pair of opposite-signed tracks identified as muons. The invariant mass of the di-muon is required to be within the range $60 < M_{\mu\mu} < 120$ GeV/c^2. For each muon track, the fiducial requirements are $p_{\mathrm{T}} > 20$ GeV/c

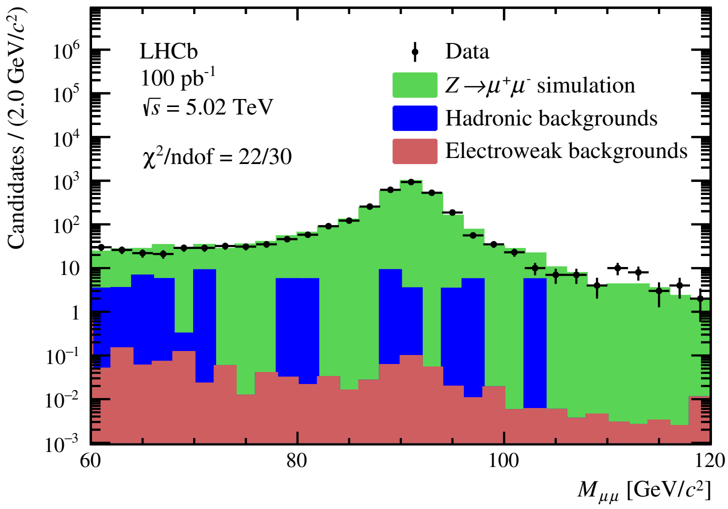

Figure 1. Mass distribution of the $Z\to\mu^+\mu^-$ signal candidates. The data are overlaid with model of the signal and background models. The signal component is scaled such that the sum of the signal and background matches the integral of the data.

and pseudorapidity in the range $2.0 < \eta < 4.5$. The muons are required to have momentum measurements with relative uncertainties below 10%. In total, 3265 $Z\to\mu^+\mu^-$ candidates meet these selection criteria, and the distribution of the di-muon invariant mass for the selected candidates is shown in figure 1.

The background contribution from decays of heavy-flavour hadrons is estimated using two control samples. These samples are used as two independent background determinations, which allow for cross-checking with each other. Tracks from heavy-flavour decays degrade the primary vertex (PV) fit quality when included in the PV fit, since heavy-flavour hadrons travel a finite distance before decaying. Hence, the first control sample is obtained by applying a requirement that the selected candidate have a PV with a low fit quality ($\chi^2 > 95$). Additionally, muons produced from semileptonic decays of heavy flavour hadrons are less isolated. The variable I_μ is defined as the ratio of the muon p_T to the vector sum of the p_T of all charged particles in a cone of size $R = \sqrt{(\Delta\eta)^2 + (\Delta\phi)^2} < 0.5$ around the muon. The second control sample is selected by requiring that the two muons are not spatially isolated ($I_\mu < 0.91$) from the rest of the event.

The yields of these two control samples are determined from a fit to the di-muon invariant mass distributions, using an exponential function. From the fitting results in appendix A, it can be observed that statistical uncertainty is the primary source of uncertainty in this estimation. The heavy-flavour background is concentrated at low mass ($50 < M_{\mu\mu} < 70\,\mathrm{GeV}/c^2$), so to obtain a larger sample and a more stable fit, the background yield is determined in the region $50 < M_{\mu\mu} < 110\,\mathrm{GeV}/c^2$. The estimated background yield is corrected for the efficiency of vertex and isolation selections, and extrapolated to the signal region ($60 < M_{\mu\mu} < 120\,\mathrm{GeV}/c^2$). The efficiency of the muon isolation (vertex quality) selection is calculated separately by applying the muon isolation requirement (vertex quality requirement) to the first (second) control sample. The background contributions estimated using these two independent samples are con-

Background	Estimation	Events	Fraction
Heavy flavour ($b\bar{b}$, $c\bar{c}$)	data-driven	65 ± 51	2.0×10^{-2}
Hadron misidentification	data-driven	0.20 ± 0.10	6.0×10^{-5}
$Z \to \tau^+\tau^-$	Simulation	0.39 ± 0.12	1.2×10^{-4}
WZ/ZZ	Simulation	0.25 ± 0.04	7.7×10^{-5}
WW	Simulation	0.19 ± 0.02	5.8×10^{-5}
$t\bar{t}$	Simulation	0.14 ± 0.10	4.4×10^{-5}
Total		66 ± 51	2.0×10^{-2}

Table 1. Summary of the background composition in the $Z \to \mu^+\mu^-$ data sample of candidates satisfying the signal selection.

sistent, and the average value is taken as the background contribution from the heavy flavour decay process, which is determined to be $(2.0 \pm 1.6) \times 10^{-2}$ for the selected $Z \to \mu^+\mu^-$ sample.

The contribution from the combinatorial background including misidentified hadrons and B-$\bar{B}$ mixing is estimated using pairs of same-sign muons in the data. In the same-sign events, a muon from heavy flavour decay combined with a misidentified hadron are expected to make sizable contributions. After removing the contribution from heavy flavour processes, the contribution from misidentified hadrons is determined to be $(6.0 \pm 3.0) \times 10^{-5}$, which is negligible. The electroweak background contributions from the $t\bar{t}$, W^+W^-, $W^\pm Z$, ZZ and $Z \to \tau^+\tau^-$ processes are estimated to be $(4.4 \pm 2.9) \times 10^{-5}$, $(5.8 \pm 0.7) \times 10^{-5}$, $(1.8 \pm 0.5) \times 10^{-5}$, $(5.9 \pm 1.2) \times 10^{-5}$ and $(1.2 \pm 0.4) \times 10^{-4}$ from the simulation, with LO to NNLO correction factors determined with the MCFM [66] package.

In summary, the total background contribution to the $Z \to \mu^+\mu^-$ sample in the mass range $60 < M_{\mu\mu} < 120\,\mathrm{GeV}/c^2$ is determined to be $(2.0 \pm 1.6) \times 10^{-2}$ and the background composition of the candidate sample is summarised in table 1.

4 Cross-section determination

Only single-differential cross-section measurements are performed due to the limited sample yields. The differential cross-section is measured as a function of y^Z, p_{T}^Z and ϕ_η^* [67], which is defined as

$$\phi_\eta^* = \tan\left[(\pi - \Delta\phi^{\ell\ell})/2\right]\sin(\theta_\eta^*), \tag{4.1}$$

where $\Delta\phi^{\ell\ell}$ represents the difference in the azimuthal angle between the two muons in the laboratory frame. The variable θ_η^* is defined by $\cos(\theta_\eta^*) = \tanh[(\eta^- - \eta^+)/2]$, with η^- and η^+ denoting the pseudorapidities of the negatively and positively charged muons in the laboratory frame. The observable ϕ_η^* probes similar physics as the transverse momentum p_{T}^Z, but is measured with near-perfect resolution.

The integrated cross-section is obtained by integrating over all bins, which are chosen based on the detector resolution and sample size. The differential cross section in a generic

JHEP02(2024)070

variable a is defined as

$$\frac{d\sigma_{Z\to\mu^+\mu^-}}{da}(i) = \frac{N_Z(i)\cdot f^Z_{FSR}(i)}{\mathcal{L}\cdot\varepsilon^Z(i)\cdot\Delta a(i)}, \tag{4.2}$$

where the generic variable a represents the observable y^Z, p_{T}^Z or ϕ^*_η, the index i indicates the bin of the variable under study, $N_Z(i)$ is the signal yield in bin i after background subtraction, $f^Z_{FSR}(i)$ is the FSR correction factor (as discussed in section 4.3), $\mathcal{L}$ is the integrated luminosity, $\Delta a(i)$ is the bin width for the i-th bin (as presented in tables 3 to 5 in appendix B), and $\varepsilon^Z(i)$ is the total efficiency in the i-th bin.

To account for detector misalignment effects, the Z mass peak position and resolution in simulated events are corrected to be compatible with the data, using momentum scaling and smearing factors [68]. The impact from this correction on the integrated cross-section measurement is found to be negligible.

4.1 Efficiency

The selection efficiencies are determined for the muon tracking, identification and trigger requirements. These are derived using the $Z\to\mu^+\mu^-$ data and a tag-and-probe method [69].

In the determination of the tracking efficiency, a particle reconstructed in all the tracking subdetectors, and fulfilling the muon trigger and muon identification requirements, is used as the tag. An object reconstructed by combining hits in the muon stations and the TT downstream tracking stations, denoted as a MuonTT track, then acts as the probe. As described in ref. [69], the tracking efficiency is calculated as the fraction of probe candidates matched with a reconstructed track. However, the precision of the measured tracking efficiency is limited by the low number of Z boson candidates in the data sample. In this analysis, we therefore use the tracking efficiency $\varepsilon^{\mathrm{MC},5.02}_{\mathrm{Tracking}}$ found from the 5.02 TeV $Z\to\mu^+\mu^-$ simulation, and apply a correction to this using a scale factor determined using the tag-and-probe method in the 13 TeV analysis [32], as

$$\varepsilon^{\mathrm{Data},5.02}_{\mathrm{Tracking}} = \varepsilon^{\mathrm{MC},5.02}_{\mathrm{Tracking}} \times \frac{\varepsilon^{\mathrm{Data},13}_{\mathrm{Tracking}}}{\varepsilon^{\mathrm{MC},13}_{\mathrm{Tracking}}}. \tag{4.3}$$

The muon identification efficiency determination is affected by statistical fluctuations similarly to the tracking efficiency, and the same treatment is applied.

The efficiency of the muon trigger is determined with the tag-and-probe method, where a tag particle is chosen from a particle reconstructed in all tracking subdetectors, which must be identified and triggered as a muon. The probe particle must pass all selection requirements used in the analysis apart from the trigger requirements. The invariant mass of tag and probe particles is further required to be within the range [60,120] GeV/c^2, and the azimuthal separation, $|\Delta\phi|$, greater than 2.7 radians. The efficiency is computed as the ratio of the number of probes meeting the muon trigger criteria to the total number of probes.

After correcting the muon tracking efficiency using eq. (4.3) and applying this correction method to the muon identification efficiency in a similar way, the determined muon tracking reconstruction efficiency $\varepsilon^{\mu^\pm}_{\mathrm{Track}}$, identification efficiency $\varepsilon^{\mu^\pm}_{\mathrm{ID}}$ and trigger efficiency $\varepsilon^{\mu^\pm}_{\mathrm{Trig}}$ vary

JHEP02(2024)070

between 94% and 98%, 90% and 97%, 62% and 85% respectively. The efficiencies measured as a function of muon pseudorapidity are presented in appendix C.

This measurement follows the efficiency correction method employed in the 13 TeV analysis [32], which involved a one-dimensional efficiency correction based solely on the muon pseudorapidity. To investigate whether any additional dependencies of efficiencies were overlooked or if the results could be entirely attributed to the 1-D correction, a so-called closure test was performed: the number of reconstructed events in simulation is corrected using the efficiencies determined in simulation, then compared to the true number of events for each of the differential distributions. The differences between this correction method and the true information from the simulation is considered as a source of systematic uncertainty (as discussed in section 5).

The Z event selection efficiency is derived from the muon efficiencies $\varepsilon_{\text{Track}}$, ε_{ID}, $\varepsilon_{\text{Trig}}$ following

$$\varepsilon^{Z} = (\varepsilon^{\mu}_{\text{Track}} \cdot \varepsilon^{\mu}_{\text{Track}}) \cdot (\varepsilon^{\mu}_{\text{ID}} \cdot \varepsilon^{\mu}_{\text{ID}}) \cdot \left(\varepsilon^{\mu}_{\text{Trig}} + \varepsilon^{\mu}_{\text{Trig}} - \varepsilon^{\mu}_{\text{Trig}} \cdot \varepsilon^{\mu}_{\text{Trig}}\right). \tag{4.4}$$

4.2 Bin migration correction

The detector resolution causes migration between kinematic bins. Due to the good angular resolution of the LHCb detector, negligible migration effects are observed among y^Z and ϕ^*_η bins. Hence, it is unnecessary to correct for migration effects on the number of events in each bin of y^Z and ϕ^*_η for the cross-section measurement.

To assess the necessity of correcting the p_{T}^{Z} measurement for bin migrations at the reconstruction level, the ratio of the p_{T}^{Z} distribution before and after applying a Bayesian unfolding procedure [70, 71] is calculated from data. This ratio is then compared to the ratio of the reconstructed to the generated p_{T}^{Z} distribution obtained from the simulated sample. As noticeable migration is detected, corrections for migration effects on the p_{T}^{Z} distribution are implemented using the Bayesian unfolding approach mentioned earlier.

4.3 Final state radiation correction

The measured cross-section is corrected to the Born level in QED, so that it can be directly compared with theoretical predictions. The final-state radiation (FSR) correction is developed and applied to the measurements, by comparing the ResBos [57] predictions with and without the implementation of Photos [54], which corrects the quantities of muons after final state radiation to the Born level. The FSR corrections in bins of y^Z, p_{T}^{Z} and ϕ^*_η are shown in figure 2. The corrections for single-differential cross-section measurements are also presented in appendix B.

5 Systematic uncertainties

The systematic uncertainties considered in the present measurement include the background estimation, the calibration of the momentum scale, the efficiency determination, the bin migration correction, the results of efficiency closure tests, the FSR correction, and the measurement of the integrated luminosity.

The determination of the heavy flavour background uses the averaged yield between two methods as the background contribution. The associated uncertainty is calculated

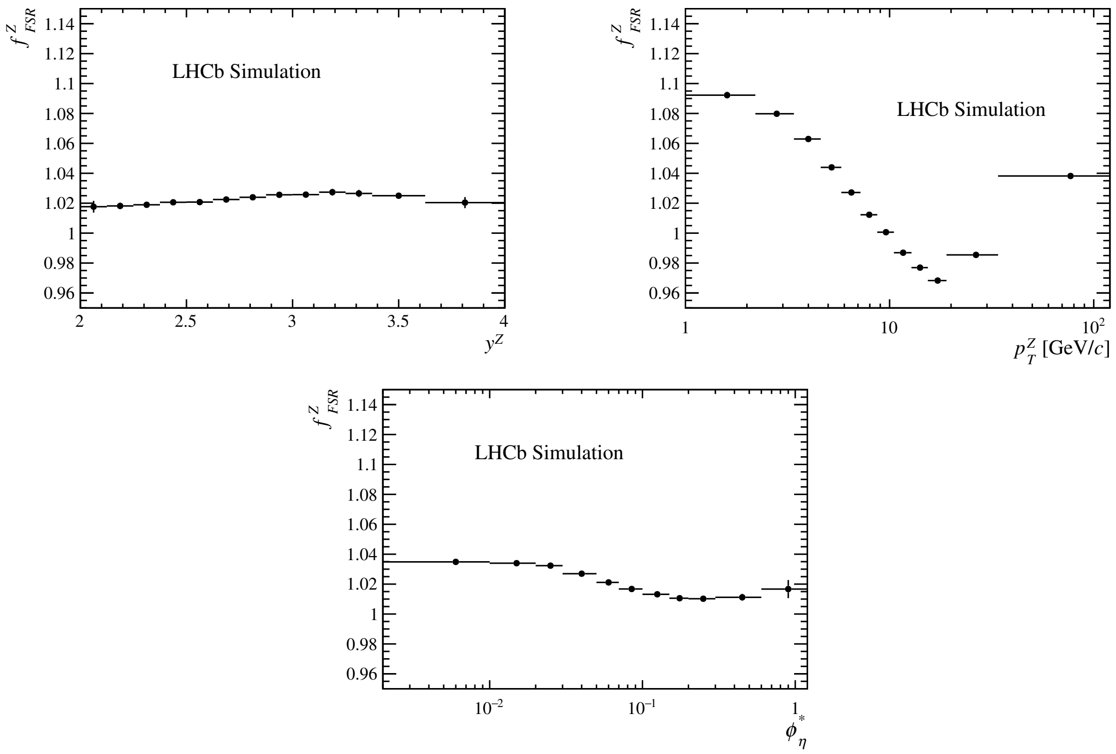

Figure 2. Final state radiation correction estimated for the (top-left) y^Z, (top-right) p_{T}^Z, and (bottom) ϕ_η^* differential cross-section measurements. The error bars represent the total (statistical and systematic) uncertainties.

as the discrepancy between the background yields obtained from the two control samples. Additionally, a systematic uncertainty is introduced by varying the mass region and selection requirements of the control samples. The hadron misidentification and other backgrounds are estimated from the data and simulation, with the statistical uncertainties being treated as systematic uncertainties that depend on the limited size of the same-sign data and simulation samples. The systematic uncertainties on the $t\bar{t}$, W^+W^-, $W^\pm Z$, ZZ, and $Z \to \tau^+\tau^-$ components derive from the statistical uncertainties and theoretical uncertainties on the LO to NNLO correction factors. To estimate the uncertainty due to inadequate calibration of the detector, the momentum scaling and smearing correction for the simulation are studied in order to improve the modeling of the $Z \to \mu^+\mu^-$ data. Only a small fraction, less than 0.01% of events, exhibits changes when comparing the simulation before and after studying the momentum scaling and smearing. This value is conservatively assigned as the systematic uncertainty related to the detector alignment. The impact from momentum calibration uncertainty on the integrated cross-section measurement is found to be negligible. However, the alignment uncertainty is considered and added for the p_{T}^Z distribution.

The track reconstruction and identification efficiencies for high p_{T} muons are calculated using simulation and data taking at $\sqrt{s} = 13$ TeV. The systematic uncertainties are determined by the size of the 5.02 TeV simulation samples and the uncertainties are propagated from the 13 TeV results. For the trigger efficiency, which is directly measured using control samples in

Source	$\Delta\sigma$ [pb]	$\Delta\sigma/\sigma$ [%]
Luminosity	0.79	2.00
Statistical	0.70	1.77
Tracking	0.40	1.01
Efficiency Closure	0.24	0.61
Trigger	0.21	0.54
Background	0.19	0.48
Identification	0.10	0.25
FSR	0.07	0.18
Calibration	$< 4.0 \times 10^{-3}$	< 0.01
Total Systematic (excl. lumi.)	0.56	1.42

Table 2. The uncertainties for the integrated $Z \to \mu^+\mu^-$ cross-section measurement.

the 5.02 TeV data, a systematic uncertainty is assigned for variations due to the limited size of the samples studied. As studied in ref. [32], an additional systematic uncertainty is evaluated, based on the method used to determine the tracking efficiency. This is evaluated to be 0.47% which is already considered in the systematic uncertainty of the muon tracking efficiency.

To examine whether it is sufficient to perform efficiency corrections only as a function of the muon pseudorapidity variable or if the efficiency also depends on other variables such as muon p_{T}, a closure test is performed. The reconstructed event yields in simulation are adjusted using the efficiencies determined solely based on the muon pseudorapidity obtained from the simulation samples and then compared with the generated yield. The differences, which do not exhibit any systematic pattern across the differential cross-section measurement regions, are attributed as an additional source of uncertainty.

To estimate the uncertainty attributed to the bin migration correction, the p_{T}^{Z} distribution is unfolded using the so-called *Invert Approach* [72], which employs a simple inversion of the response matrix without regularisation. The deviation of the results from the *Bayesian Approach* [70, 71] is taken as a systematic uncertainty on the p_{T}^{Z} differential cross-section. The systematic uncertainty arising from the FSR correction is evaluated by comparing the default correction with one determined using the Powheg generator showered using Pythia. The differences in FSR corrections between ResBos with Photos and Powheg with Pythia are then taken into consideration as a systematic uncertainty. Regarding the data sample used, the luminosity is determined with a precision of 2.0% [43], which is quoted separately to the other sources of systematic uncertainty. The statistical and systematic uncertainties in the integrated cross-section measurement are listed in table 2. The different sources of systematic uncertainty for each bin of the differential cross-sections are summarised in tables 7 to 9 in appendix D.

6 Results

6.1 Differential cross-section results

The single differential cross-sections in regions of y^Z, p_T^Z and ϕ_η^* are shown in figure 3, together with the ratios of theoretical predictions to data. The numerical results of single differential cross-section within each bin are summarised in tables 10–12 in appendix E.

Measurements are in reasonable agreement with the different theoretical predictions. In both the lower and higher p_T^Z and ϕ_η^* region, the measurements agree with predictions from both ResBos and Powheg. For the measurement of y^Z, the theoretical predictions from the three generators are also compatible with the experimental results within the uncertainty range.

6.2 Correlation matrices

The event migration between bins causes statistical correlations, which are determined using simulation. Large correlations are found in the low-p_T^Z region and small correlations in the high-p_T^Z region, while the statistical correlations are negligible for both the y^Z and ϕ_η^* distributions.

For the differential cross-section measurements, background, alignment, efficiency closure test, and FSR uncertainties are assumed to be 50% correlated between different bins, while the luminosity uncertainty is considered to be 100% correlated. The calculated correlation matrices for the efficiencies are presented in appendix F. Large correlations between different bins are present in the p_T^Z differential cross-section measurement, but small correlations are also present between most bins for the y^Z and ϕ_η^* measurements.

6.3 Integrated cross-section results

Using the LHCb 2017 pp collision data at $\sqrt{s} = 5.02\,\text{TeV}$, the integrated Born-level Z boson production cross-section, with two muons in the final state and within the LHCb acceptance is

$$\sigma_{Z\to\mu^+\mu^-} = 39.6 \pm 0.7\,(\text{stat}) \pm 0.6\,(\text{syst}) \pm 0.8\,(\text{lumi})\ \text{pb} \tag{6.1}$$

where the uncertainties are due to statistical effects, systematic effects, and the luminosity measurement, respectively.

In this article, the Z boson is defined to also include contributions from virtual photons, and the interference between them since they cannot be distinguished experimentally. The measured results obtained for the total cross-section of the $pp \to Z \to \mu^+\mu^-$ process at 5.02 TeV in the fiducial region of the LHCb detector have been compared to the predictions obtained using MCFM with CT18NNLO and other theoretical models, including Powheg-Box with NNPDF3.1, NNPDF4.0, MSHT20, CT18, and ResBos with CT18, all of which account for both statistical and PDF uncertainties. These theoretical predictions are compared to the results in figure 4, which demonstrate a reasonable agreement.

By comparing the theoretical predictions at different center-of-mass energies provided by MCFM, with the experimental measurements previously obtained by LHCb at $\sqrt{s} = 7$, 8 and 13 TeV, as illustrated in figure 5, a good level of consistency can be observed overall.

JHEP02(2024)070

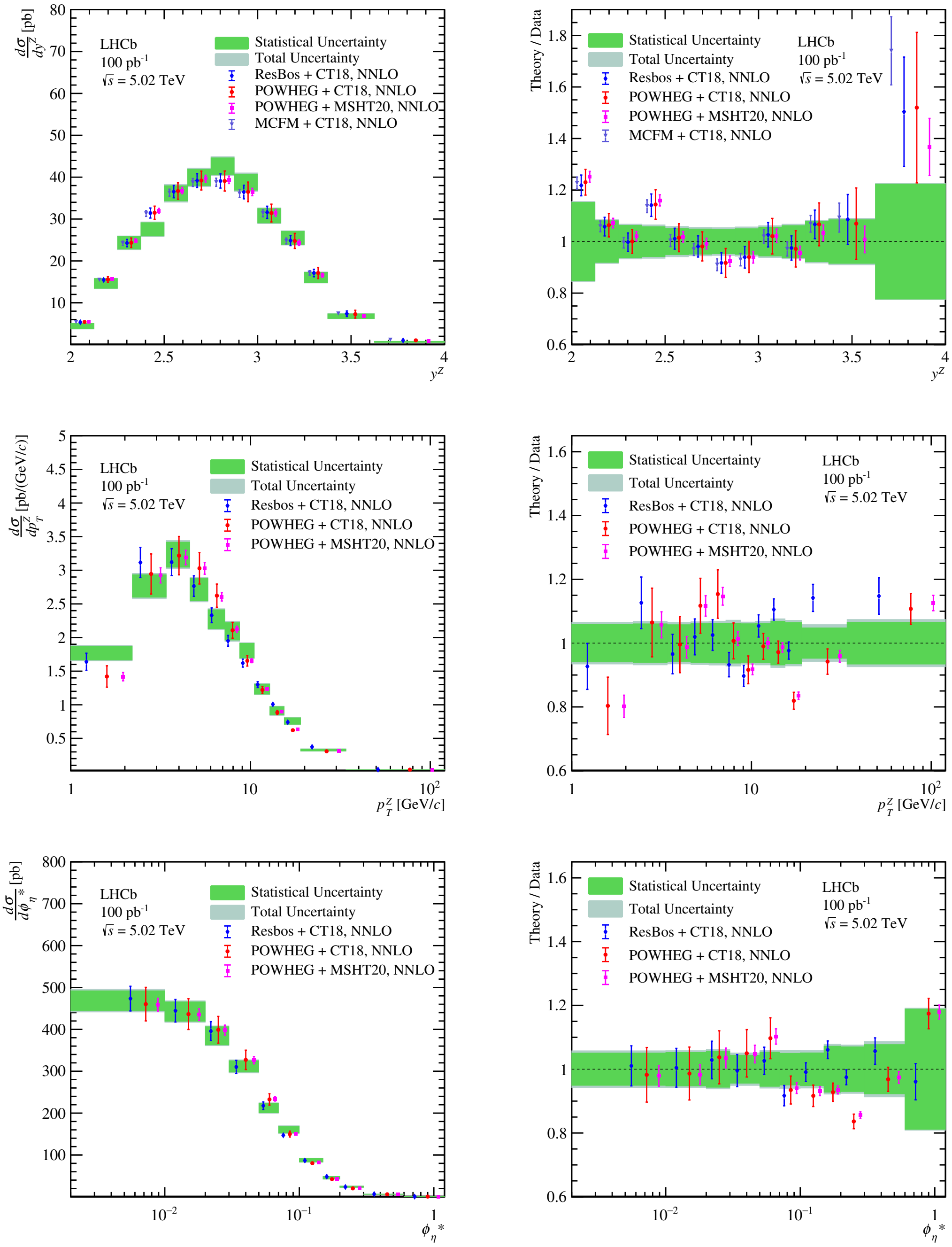

Figure 3. (Left) Measured single differential cross-section as a function of y^Z, p_{T}^{Z} and ϕ_{η}^{*} compared with different theoretical predictions. (Right) Ratio of theoretical predictions to measured values, with the horizontal bars showing the uncertainty from the PDFs. The green band, centered at unity, shows the uncertainty of the measurement.

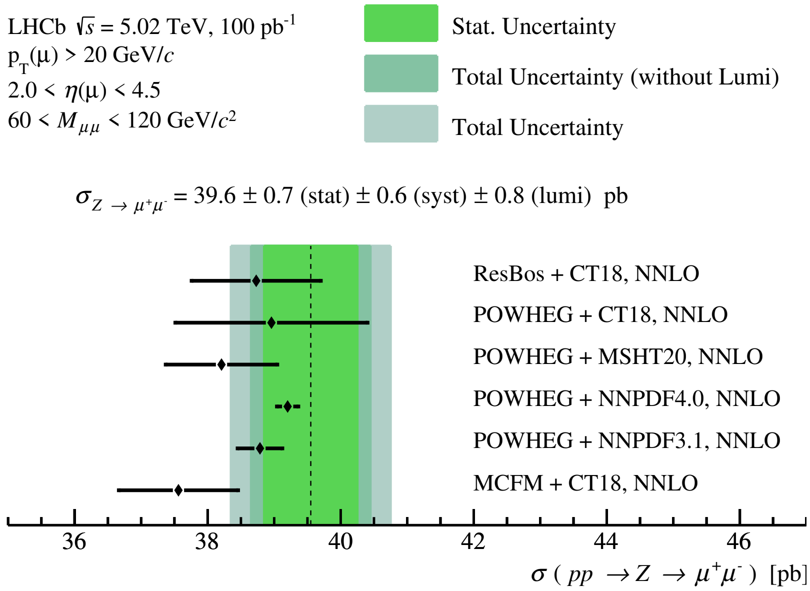

Figure 4. Comparison of the integrated cross-section, $\sigma_{Z\to\mu^+\mu^-}$, between data and theoretical predictions. The bands correspond to the data, with the inner band corresponding to the statistical uncertainty and the outer bands corresponding to the systematic uncertainty and total uncertainty.

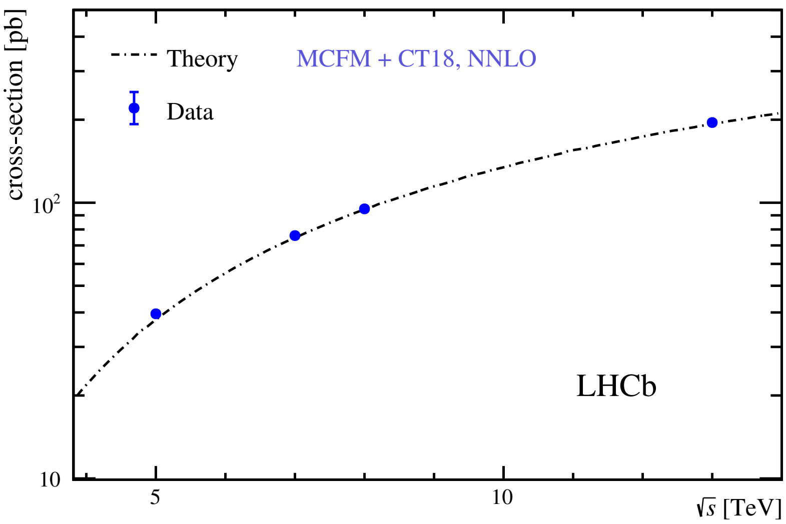

Figure 5. Measured $\sigma_{Z\to\mu^+\mu^-}$ for pp collisions, as a function of $\sqrt{s}$. The uncertainty on the data is smaller than the marker size. The data are overlaid with a curve showing the theoretical prediction.

6.4 Nuclear modification factors

The nuclear modification factors are determined based on the present measurements and those in ref. [42]. Here, the statistical and systematic uncertainties (including uncertainties due to integrated luminosity) of the cross-sections measured between pp and pPb collisions are assumed to be fully uncorrelated when being propagated to the nuclear modification factors. Efficiency and background modeling uncertainties are also treated as fully uncorrelated, owing to the very different running conditions between pp and pPb collisions such as the heavier detector contamination from the higher charged hadron multiplicities in case of pPb. All other sources of systematic uncertainty are considered to be uncorrelated, an assumption that has negligible effect to the reported results.

The unique forward geometry coverage allows the LHCb detector to probe nPDFs at very small Bjorken-x ($10^{-4} < x < 10^{-3}$). The nuclear modification factors can be calculated using the pp cross-section measured here together with the Z boson production cross-section in pPb collisions measured in ref. [42]. The nuclear modification factors are defined as the ratio of the Z boson production cross-sections between pPb and pp collisions under the same muon rapidity acceptance. Due to the asymmetric beam energy in the pPb centre-of-mass frame, the muon rapidity acceptance ($2.0 < \eta < 4.5$) becomes $1.53 < y^*_\mu < 4.03$ in case of the forward collisions, and $-4.97 < y^*_\mu < -2.47$ in case of backward collisions, where y^*_μ represents the muon rapidity in the centre-of-mass frame. The two rapidity quantities are identical in pp collisions, $\eta_\mu \equiv y^*_\mu$, due to the symmetric beam energy. Forward collisions refer to the proton beam entering the LHCb detector along the positive direction of the z axis, while backward collisions correspond to the proton beam going in the opposite direction.

The cross-sections of the pPb collisions measured under different rapidity acceptances need to be corrected before being used to calculate the nuclear modification factors. The $k_{p\text{Pb}}$ factor corrects for the different η acceptance between pPb and pp collisions and can be calculated using Powheg with the proton PDF set CTEQ6.1 [73],

$$k^{\text{F}}_{p\text{Pb}} = \frac{\sigma_{(pp,\ 2.0<\eta<4.5)}}{\sigma_{(pp,\ 1.53<\eta<4.03)}} = 0.706 \pm 0.002, \tag{6.2}$$

and

$$k^{\text{B}}_{p\text{Pb}} = \frac{\sigma_{(pp,\ 2.0<\eta<4.5)}}{\sigma_{(pp,\ -4.97<\eta<-2.47)}} = 1.518 \pm 0.003, \tag{6.3}$$

for forward and backward collisions, respectively. The integrated nuclear modification factors can then be defined as follows

$$R^{\text{F}}_{p\text{Pb}} = k^{\text{F}}_{p\text{Pb}} \cdot \frac{\sigma_{(p\text{Pb},\ 1.53<y^*_\mu<4.03)}}{208 \cdot \sigma_{(pp,\ 2.0<\eta<4.5)}}, \tag{6.4}$$

and

$$R^{\text{B}}_{p\text{Pb}} = k^{\text{B}}_{p\text{Pb}} \cdot \frac{\sigma_{(p\text{Pb},\ -4.97<y^*_\mu<-2.47)}}{208 \cdot \sigma_{(pp,\ 2.0<\eta<4.5)}}, \tag{6.5}$$

for forward and backwards pPb collisions, respectively, with 208 being the number of binary nucleon-nucleon collisions in pPb collisions. The quantity $\sigma_{(p\text{Pb},\ 1.53<y^*_\mu<4.03)}$ is measured to be $13.5^{+5.4}_{-4.0}\,(\text{stat}) \pm 1.2\,(\text{syst})$ nb, and $\sigma_{(p\text{Pb},\ -4.97<y^*_\mu<-2.47)}$ is measured to be $10.7^{+8.4}_{-5.1}\,(\text{stat}) \pm 1.0\,(\text{syst})$ nb [42].

JHEP02(2024)070

The nuclear modification factors are calculated to be

$$R_{pPb}^{\mathrm{F}} = 1.2^{+0.5}_{-0.3}\,(\mathrm{stat}) \pm 0.1\,(\mathrm{syst})$$

for the forward collisions, and

$$R_{pPb}^{\mathrm{B}} = 3.6^{+1.6}_{-0.9}\,(\mathrm{stat}) \pm 0.2\,(\mathrm{syst})$$

for the backward collisions. The large statistical uncertainties are due to the small size of the pPb data sample.

Based on the theoretical prediction of the cross-sections from ref. [42] derived using FEWZ [74] at NNLO with EPS09 nPDFs [40] and MSTW08 PDFs [41], the predicted $R_{p\mathrm{Pb}}$ can be derived as $R_{p\mathrm{Pb}}^{\mathrm{F,\,theo.}} = 0.906^{+0.002}_{-0.007}$ and $R_{pPb}^{\mathrm{B,\,theo.}} = 0.929^{+0.011}_{-0.028}$ for the forward and backward collisions, respectively. The measurement and theoretical prediction agree within the uncertainties in the forward region, whereas a $2.86\,\sigma$ tension between the measured result and the prediction is seen in the backward region. However, due to the limited size of the pPb sample, the tension could be caused by a statistical fluctuation.

7 Conclusion

This paper reports the first measurement of Z boson production cross-section at the centre-of-mass energy $\sqrt{s} = 5.02\,\mathrm{TeV}$, using the LHCb pp collision dataset collected in 2017. The techniques employed in this analysis closely follow those established in a previous LHCb Run 2 analysis [32]. The results show reasonable agreement with various predictions in the Standard Model. Combining this measurement with the previous inclusive Z production result in pPb collisions at $\sqrt{s_{NN}} = 5.02\,\mathrm{TeV}$ [42] the nuclear modification factors in the forward and backward regions are obtained for the first time.

Acknowledgments

We express our gratitude to our colleagues in the CERN accelerator departments for the excellent performance of the LHC. We thank the technical and administrative staff at the LHCb institutes. We acknowledge support from CERN and from the national agencies: CAPES, CNPq, FAPERJ and FINEP (Brazil); MOST and NSFC (China); CNRS/IN2P3 (France); BMBF, DFG and MPG (Germany); INFN (Italy); NWO (Netherlands); MNiSW and NCN (Poland); MEN/IFA (Romania); MICINN (Spain); SNSF and SER (Switzerland); NASU (Ukraine); STFC (United Kingdom); DOE NP and NSF (U.S.A.). We acknowledge the computing resources that are provided by CERN, IN2P3 (France), KIT and DESY (Germany), INFN (Italy), SURF (Netherlands), PIC (Spain), GridPP (United Kingdom), CSCS (Switzerland), IFIN-HH (Romania), CBPF (Brazil), Polish WLCG (Poland) and NERSC (U.S.A.). We are indebted to the communities behind the multiple open-source software packages on which we depend. Individual groups or members have received support from ARC and ARDC (Australia); Minciencias (Colombia); AvH Foundation (Germany); EPLANET, Marie Skłodowska-Curie Actions, ERC and NextGenerationEU (European Union); A*MIDEX, ANR, IPhU and Labex P2IO, and Région Auvergne-Rhône-Alpes (France); Key

JHEP02(2024)070

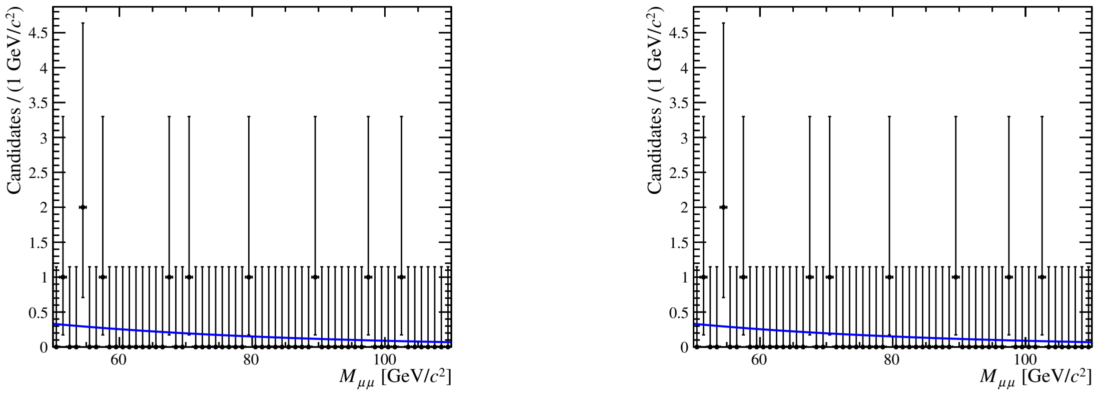

Figure 6. Invariant mass distributions of heavy-flavour samples with (left) PV fit quality $\chi^2 > 95$ and (right) $I_\mu < 91\%$ applied to both muons. Only statistical uncertainties are shown.

Research Program of Frontier Sciences of CAS, CAS PIFI, CAS CCEPP, Fundamental Research Funds for the Central Universities, and Sci. & Tech. Program of Guangzhou (China); GVA, XuntaGal, GENCAT, Inditex, InTalent and Prog. Atracción Talento, CM (Spain); SRC (Sweden); the Leverhulme Trust, the Royal Society and UKRI (United Kingdom).

A Invariant mass fitting results for background

To estimate the signal yield for heavy-flavour background-dominated samples, an exponential function is used to fit the dimuon invariant mass distributions in the region of $50-110\,\text{GeV}/c^2$, using a binned likelihood method. The distribution of selected candidates and fitted results are shown in figure 6. The fit result is then extrapolated to determine the background contribution in the mass region of $60-120\,\text{GeV}/c^2$.

B Final state radiation corrections

Tabulated results of final state radiation corrections used in the single differential cross-section measurements are presented in tables 3 to 5.

JHEP02(2024)070

y^Z	Correction
[2.000, 2.125]	1.018 ± 0.004 ± 0.092
[2.125, 2.250]	1.018 ± 0.002 ± 0.000
[2.250, 2.375]	1.019 ± 0.002 ± 0.006
[2.375, 2.500]	1.021 ± 0.002 ± 0.057
[2.500, 2.625]	1.021 ± 0.001 ± 0.046
[2.625, 2.750]	1.022 ± 0.001 ± 0.122
[2.750, 2.875]	1.024 ± 0.002 ± 0.009
[2.875, 3.000]	1.026 ± 0.002 ± 0.162
[3.000, 3.125]	1.026 ± 0.002 ± 0.070
[3.125, 3.250]	1.027 ± 0.002 ± 0.128
[3.250, 3.375]	1.027 ± 0.002 ± 0.011
[3.375, 3.625]	1.025 ± 0.002 ± 0.023
[3.625, 4.000]	1.020 ± 0.004 ± 0.001

Table 3. Final state radiation correction used in the y^Z cross-section measurement. The first uncertainty is statistical and the second is systematic.

p_T^Z [GeV/c]	Correction
[0.0, 2.2]	1.092 ± 0.002 ± 0.020
[2.2, 3.4]	1.080 ± 0.002 ± 0.018
[3.4, 4.6]	1.063 ± 0.002 ± 0.003
[4.6, 5.8]	1.044 ± 0.002 ± 0.015
[5.8, 7.2]	1.027 ± 0.002 ± 0.029
[7.2, 8.7]	1.012 ± 0.002 ± 0.025
[8.7, 10.5]	1.001 ± 0.002 ± 0.003
[10.5, 12.8]	0.987 ± 0.002 ± 0.006
[12.8, 15.4]	0.977 ± 0.002 ± 0.010
[15.4, 19.0]	0.968 ± 0.002 ± 0.005
[19.0, 34.0]	0.985 ± 0.001 ± 0.000
[34.0, 120.0]	1.038 ± 0.002 ± 0.000

Table 4. Final state radiation correction used in the p_T^Z cross-section measurement. The first uncertainty is statistical and the second is systematic.

JHEP02(2024)070

ϕ^*_η	Correction
[0.00, 0.01]	1.035 ± 0.002 ± 3.802
[0.01, 0.02]	1.034 ± 0.002 ± 0.919
[0.02, 0.03]	1.032 ± 0.002 ± 1.384
[0.03, 0.05]	1.027 ± 0.001 ± 0.878
[0.05, 0.07]	1.021 ± 0.002 ± 1.060
[0.07, 0.10]	1.017 ± 0.002 ± 0.378
[0.10, 0.15]	1.013 ± 0.002 ± 0.220
[0.15, 0.20]	1.011 ± 0.002 ± 0.288
[0.20, 0.30]	1.010 ± 0.002 ± 0.236
[0.30, 0.60]	1.011 ± 0.002 ± 0.039
[0.60, 1.20]	1.017 ± 0.006 ± 0.001

Table 5. Final state radiation correction used in the ϕ^*_η cross-section measurement. The first uncertainty is statistical and the second is systematic.

JHEP02(2024)070

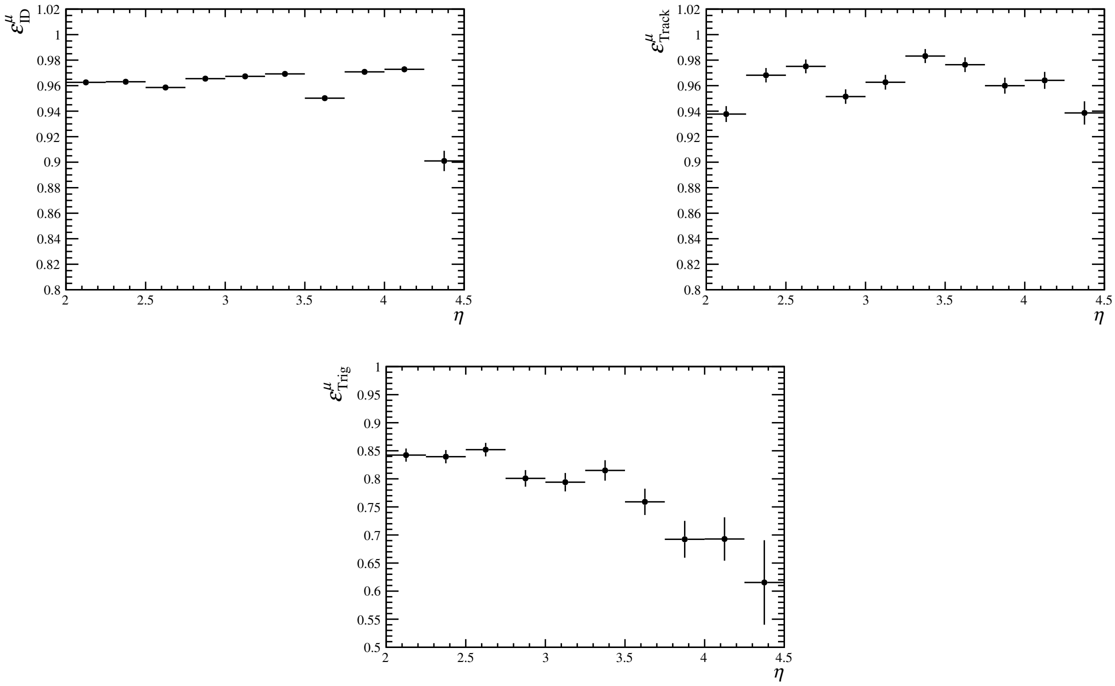

Figure 7. Muon tracking, identification and trigger efficiency as a function of pseudorapidity, estimated from the data and simulation at 5.02 TeV and 13 TeV.

η	$\varepsilon^{\mu}_{\mathrm{Track}}$ [%]	$\varepsilon^{\mu}_{\mathrm{ID}}$ [%]	$\varepsilon^{\mu}_{\mathrm{Trig}}$ [%]
[2.00, 2.25]	93.77	96.26	84.23
[2.25, 2.50]	96.82	96.30	83.95
[2.50, 2.75]	97.51	95.85	85.20
[2.75, 3.00]	95.14	96.55	80.08
[3.00, 3.25]	96.26	96.73	79.41
[3.25, 3.50]	98.32	96.92	81.50
[3.50, 3.75]	97.64	95.02	75.90
[3.75, 4.00]	96.00	97.08	69.23
[4.00, 4.25]	96.41	97.28	69.29
[4.25, 4.50]	93.86	90.10	61.54

Table 6. The muon tracking, muon identification and trigger efficiency in each pseudorapidity bin.

C Efficiency

Results of muon efficiencies used in the total Z boson efficiency calculation are presented in figure 7 and table 6.

JHEP02(2024)070

y^Z	Efficiency	Background	FSR	Closure
$[2.000,\ 2.125]$	1.42	0.04	2.10	0.45
$[2.125,\ 2.250]$	1.37	0.77	0.00	0.31
$[2.250,\ 2.375]$	1.32	0.62	0.02	0.34
$[2.375,\ 2.500]$	1.31	1.47	0.21	0.67
$[2.500,\ 2.625]$	1.32	1.42	0.13	1.17
$[2.625,\ 2.750]$	1.33	0.28	0.30	0.92
$[2.750,\ 2.875]$	1.36	0.52	0.02	0.89
$[2.875,\ 3.000]$	1.40	0.39	0.42	1.13
$[3.000,\ 3.125]$	1.46	0.51	0.23	0.68
$[3.125,\ 3.250]$	1.56	0.00	0.50	0.58
$[3.250,\ 3.375]$	1.63	0.00	0.07	1.01
$[3.375,\ 3.625]$	1.85	1.14	0.34	0.85
$[3.625,\ 4.000]$	2.23	0.00	0.21	0.80

Table 7. Systematic uncertainties on the single differential cross-sections in bins of y^Z, presented in percentage.

p_{T}^{Z} [GeV/c]	Efficiency	Background	FSR	Closure	Calibration	Migration
$[0.0,\ 2.2]$	1.42	0.56	1.15	0.43	0.13	0.54
$[2.2,\ 3.4]$	1.41	0.50	0.64	0.37	0.40	1.73
$[3.4,\ 4.6]$	1.43	0.09	0.09	0.50	0.28	1.66
$[4.6,\ 5.8]$	1.40	0.04	0.55	0.05	0.74	1.18
$[5.8,\ 7.2]$	1.43	0.25	1.27	0.12	0.91	0.36
$[7.2,\ 8.7]$	1.38	0.60	1.19	2.11	0.59	0.02
$[8.7,\ 10.5]$	1.44	0.20	0.14	0.50	0.54	0.04
$[10.5,\ 12.8]$	1.39	1.34	0.48	0.97	0.31	0.03
$[12.8,\ 15.4]$	1.39	2.00	1.11	0.18	0.36	0.01
$[15.4,\ 19.0]$	1.39	1.10	0.71	1.16	0.17	0.00
$[19.0,\ 34.0]$	1.37	1.09	0.09	1.97	0.10	0.00
$[34.0,\ 120.0]$	1.36	1.03	0.31	2.18	0.16	0.00

Table 8. Systematic uncertainties on the single differential cross-sections in bins of p_{T}^{Z}, presented in percentage.

D Summary of systematic uncertainties

The summarised systematic uncertainties for single differential cross-sections are shown in tables 7 to 9.

JHEP02(2024)070

ϕ^*_η	Efficiency	Background	FSR	Closure
[0.00, 0.01]	1.41	1.10	0.81	0.01
[0.01, 0.02]	1.42	0.43	0.21	0.00
[0.02, 0.03]	1.41	0.14	0.36	0.12
[0.03, 0.05]	1.42	0.52	0.28	0.45
[0.05, 0.07]	1.41	0.01	0.50	0.44
[0.07, 0.10]	1.39	0.29	0.24	2.22
[0.10, 0.15]	1.39	1.45	0.25	0.81
[0.15, 0.20]	1.39	0.82	0.63	1.35
[0.20, 0.30]	1.38	0.77	0.97	1.00
[0.30, 0.60]	1.37	1.45	0.61	2.72
[0.60, 1.20]	1.38	0.09	0.13	2.13

Table 9. Systematic uncertainties on the single differential cross-sections in bins of ϕ^*_η, presented in percentage.

y^Z	$d\sigma(Z\to\mu^+\mu^-)/dy^Z$ [pb]
[2.000, 2.125]	4.4 $\pm$ 0.7 $\pm$ 0.1 $\pm$ 0.1
[2.125, 2.250]	14.6 $\pm$ 1.2 $\pm$ 0.2 $\pm$ 0.3
[2.250, 2.375]	24.3 $\pm$ 1.5 $\pm$ 0.4 $\pm$ 0.5
[2.375, 2.500]	27.5 $\pm$ 1.6 $\pm$ 0.6 $\pm$ 0.6
[2.500, 2.625]	36.1 $\pm$ 1.8 $\pm$ 0.8 $\pm$ 0.7
[2.625, 2.750]	39.9 $\pm$ 2.0 $\pm$ 0.7 $\pm$ 0.8
[2.750, 2.875]	42.6 $\pm$ 2.0 $\pm$ 0.7 $\pm$ 0.9
[2.875, 3.000]	38.8 $\pm$ 1.9 $\pm$ 0.7 $\pm$ 0.8
[3.000, 3.125]	30.8 $\pm$ 1.7 $\pm$ 0.5 $\pm$ 0.6
[3.125, 3.250]	25.5 $\pm$ 1.6 $\pm$ 0.4 $\pm$ 0.5
[3.250, 3.375]	16.0 $\pm$ 1.3 $\pm$ 0.3 $\pm$ 0.3
[3.375, 3.625]	6.8 $\pm$ 0.6 $\pm$ 0.2 $\pm$ 0.1
[3.625, 4.000]	0.7 $\pm$ 0.2 $\pm$ 0.0 $\pm$ 0.0

Table 10. Measured single differential cross-sections in bins of y^Z. The first uncertainty is statistical, the second systematic, and the third is from the uncertainty on the integrated luminosity.

E Numerical results of single differential cross-sections

The measured single differential cross-sections in bins of y^Z, p_{T}^Z and ϕ^*_η are presented in tables 10 to 12.

p_{T}^{Z} [GeV/c]	$d\sigma(Z\to\mu^+\mu^-)/dp_{\mathrm{T}}^{Z}$ [pb/(GeV/c)]						
[0.0, 2.2]	1.769	±	0.105	±	0.036	±	0.035
[2.2, 3.4]	2.77	±	0.17	±	0.07	±	0.06
[3.4, 4.6]	3.23	±	0.19	±	0.07	±	0.06
[4.6, 5.8]	2.71	±	0.17	±	0.06	±	0.05
[5.8, 7.2]	2.27	±	0.14	±	0.05	±	0.05
[7.2, 8.7]	2.09	±	0.13	±	0.06	±	0.04
[8.7, 10.5]	1.806	±	0.110	±	0.030	±	0.036
[10.5, 12.8]	1.234	±	0.076	±	0.028	±	0.025
[12.8, 15.4]	0.911	±	0.063	±	0.025	±	0.018
[15.4, 19.0]	0.759	±	0.050	±	0.017	±	0.015
[19.0, 34.0]	0.328	±	0.016	±	0.009	±	0.007
[34.0, 120.0]	0.0325	±	0.0021	±	0.0009	±	0.0007

Table 11. Measured single differential cross-sections in bins of p_{T}^{Z}. The first uncertainty is statistical, the second systematic, and the third is due to the luminosity.

ϕ_{η}^{*}	$d\sigma(Z\to\mu^+\mu^-)/d\phi_{\eta}^{*}$ [pb]						
[0.00, 0.01]	468.5	±	23.8	±	9.2	±	9.4
[0.01, 0.02]	442.4	±	23.4	±	6.6	±	8.8
[0.02, 0.03]	384.6	±	21.9	±	5.6	±	7.7
[0.03, 0.05]	311.6	±	13.8	±	5.0	±	6.2
[0.05, 0.07]	212.1	±	11.5	±	3.3	±	4.2
[0.07, 0.10]	160.4	±	8.0	±	4.2	±	3.2
[0.10, 0.15]	87.63	±	4.51	±	1.91	±	1.75
[0.15, 0.20]	45.59	±	3.31	±	1.00	±	0.91
[0.20, 0.30]	24.21	±	1.70	±	0.51	±	0.48
[0.30, 0.60]	6.30	±	0.49	±	0.22	±	0.13
[0.60, 1.20]	0.571	±	0.108	±	0.015	±	0.011

Table 12. Measured single differential cross-sections in bins of ϕ_{η}^{*}. The first uncertainty is statistical, the second systematic, and the third is due to the luminosity.

JHEP02(2024)070

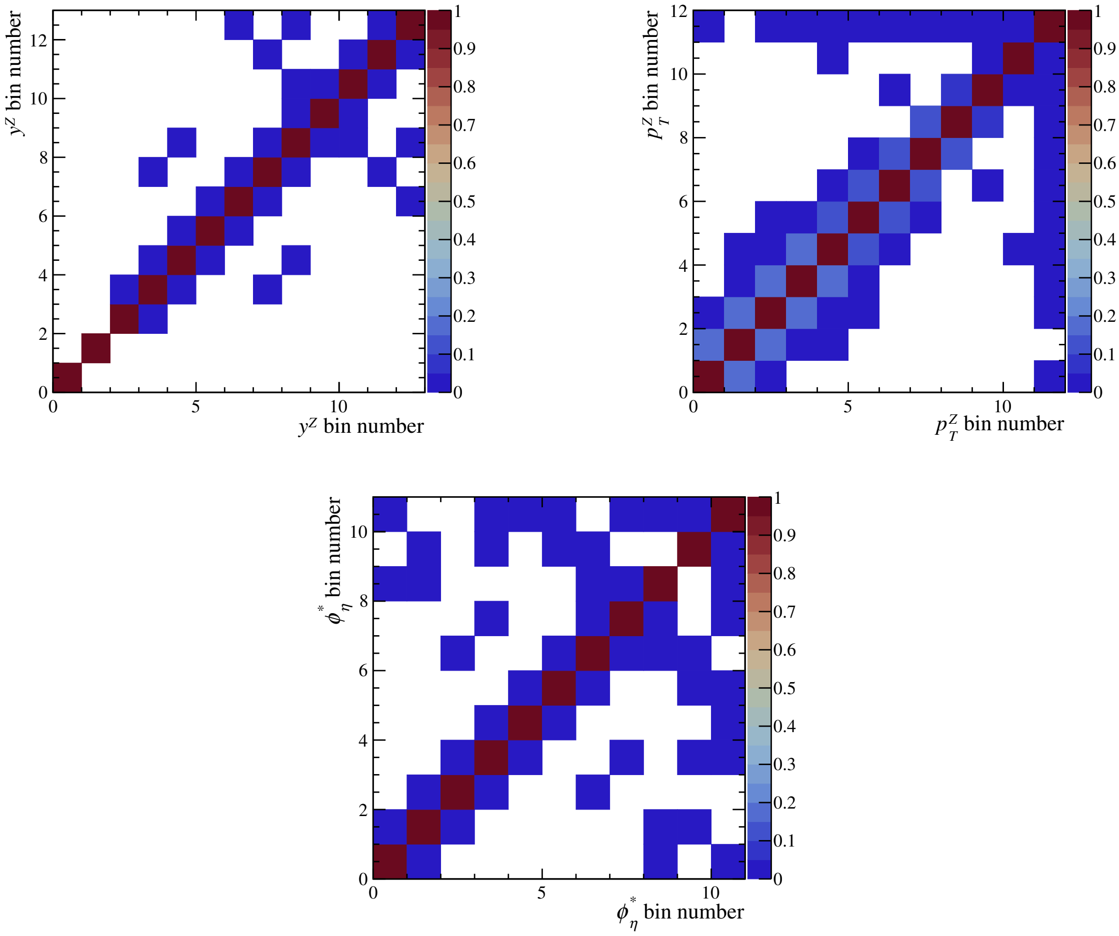

Figure 8. Statistical correlation matrices for the differential cross-section measurements as functions of (top-left) y^Z, (top-right) p_T^Z and (bottom) ϕ_η^*.

F Correlation matrices

The calculated statistical correlation matrices are shown in figure 8 and presented in tables 13 to 15. The correlation matrices for the efficiency uncertainty are shown in figure 9 for single differential cross-section measurements, and presented in tables 16 to 18.

JHEP02(2024)070

Bin	1	2	3	4	5	6	7	8	9	10	11	12	13
1	1.00												
2	0.00	1.00											
3	0.00	0.00	1.00										
4	0.00	0.00	0.00	1.00									
5	0.00	0.00	0.00	0.01	1.00								
6	0.00	0.00	0.00	0.00	0.01	1.00							
7	0.00	0.00	0.00	0.00	0.00	0.01	1.00						
8	0.00	0.00	0.00	0.00	0.00	0.00	0.01	1.00					
9	0.00	0.00	0.00	0.00	0.00	0.00	0.00	0.01	1.00				
10	0.00	0.00	0.00	0.00	0.00	0.00	0.00	0.00	0.01	1.00			
11	0.00	0.00	0.00	0.00	0.00	0.00	0.00	0.00	0.00	0.01	1.00		
12	0.00	0.00	0.00	0.00	0.00	0.00	0.00	0.00	0.00	0.00	0.02	1.00	
13	0.00	0.00	0.00	0.00	0.00	0.00	0.00	0.00	0.00	0.00	0.00	0.00	1.00

Table 13. Statistical correlation matrix for the one-dimensional y^Z measurement.

Bin	1	2	3	4	5	6	7	8	9	10	11	12
1	1.00											
2	0.16	1.00										
3	0.00	0.18	1.00									
4	0.00	0.01	0.18	1.00								
5	0.00	0.00	0.01	0.18	1.00							
6	0.00	0.00	0.00	0.01	0.14	1.00						
7	0.00	0.00	0.00	0.00	0.01	0.12	1.00					
8	0.00	0.00	0.00	0.00	0.00	0.00	0.10	1.00				
9	0.00	0.00	0.00	0.00	0.00	0.00	0.00	0.10	1.00			
10	0.00	0.00	0.00	0.00	0.00	0.00	0.00	0.00	0.05	1.00		
11	0.00	0.00	0.00	0.00	0.00	0.00	0.00	0.00	0.00	0.04	1.00	
12	0.00	0.00	0.00	0.00	0.00	0.01	0.00	0.00	0.00	0.01	0.01	1.00

Table 14. Statistical correlation matrix for the one-dimensional p_{T}^Z measurement.

JHEP02(2024)070

Bin	1	2	3	4	5	6	7	8	9	10	11
1	1.00										
2	0.01	1.00									
3	0.00	0.01	1.00								
4	0.00	0.00	0.01	1.00							
5	0.00	0.00	0.00	0.01	1.00						
6	0.00	0.00	0.00	0.00	0.00	1.00					
7	0.00	0.00	0.00	0.00	0.00	0.00	1.00				
8	0.00	0.00	0.00	0.00	0.00	0.00	0.00	1.00			
9	0.00	0.00	0.00	0.00	0.00	0.00	0.00	0.00	1.00		
10	0.00	0.00	0.00	0.00	0.00	0.00	0.00	0.00	0.00	1.00	
11	0.00	0.00	0.00	0.00	0.00	0.00	0.00	0.00	0.00	0.00	1.00

Table 15. Statistical correlation matrix for the one-dimensional ϕ^*_η measurement.

Bin	1	2	3	4	5	6	7	8	9	10	11	12	13
1	1.00												
2	0.92	1.00											
3	0.68	0.89	1.00										
4	0.56	0.74	0.93	1.00									
5	0.49	0.62	0.77	0.92	1.00								
6	0.34	0.47	0.65	0.81	0.95	1.00							
7	0.31	0.41	0.54	0.67	0.82	0.94	1.00						
8	0.19	0.28	0.40	0.53	0.69	0.81	0.93	1.00					
9	0.14	0.21	0.29	0.38	0.51	0.63	0.78	0.94	1.00				
10	0.13	0.19	0.27	0.35	0.44	0.54	0.69	0.87	0.99	1.00			
11	0.13	0.18	0.25	0.33	0.42	0.52	0.68	0.87	0.98	1.00	1.00		
12	0.16	0.22	0.29	0.37	0.46	0.57	0.72	0.89	0.99	1.00	1.00	1.00	
13	0.16	0.21	0.27	0.34	0.42	0.52	0.68	0.87	0.98	1.00	1.00	1.00	1.00

Table 16. Correlation matrix for the efficiency uncertainty of the one-dimensional y^Z measurement.

JHEP02(2024)070

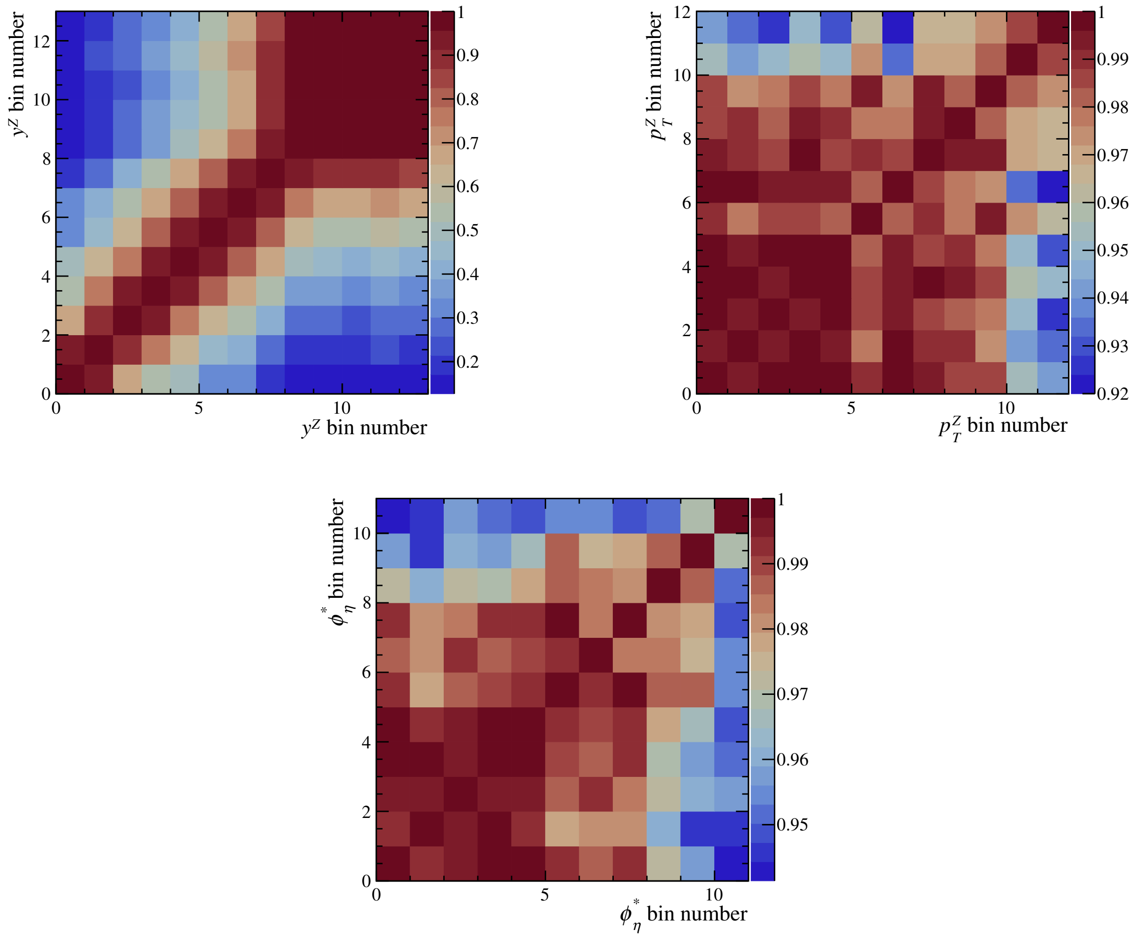

Figure 9. Correlation matrices for the efficiency uncertainties as functions of (top-left) y^Z, (top-right) p_{T}^Z and (bottom) ϕ^*_η.

JHEP02(2024)070

Bin	1	2	3	4	5	6	7	8	9	10	11	12
1	1.00											
2	1.00	1.00										
3	1.00	0.99	1.00									
4	1.00	1.00	1.00	1.00								
5	1.00	1.00	1.00	1.00	1.00							
6	0.99	0.98	0.99	0.99	0.98	1.00						
7	1.00	1.00	1.00	1.00	1.00	0.98	1.00					
8	0.99	0.99	0.99	1.00	0.99	0.99	0.99	1.00				
9	0.99	0.99	0.98	0.99	0.99	0.98	0.98	0.99	1.00			
10	0.98	0.98	0.98	0.99	0.98	0.99	0.97	0.99	0.98	1.00		
11	0.96	0.94	0.95	0.96	0.95	0.97	0.93	0.97	0.97	0.98	1.00	
12	0.94	0.93	0.93	0.95	0.93	0.96	0.92	0.97	0.97	0.98	0.99	1.00

Table 17. Correlation matrix for the efficiency uncertainty of the one-dimensional p_{T}^{Z} measurement.

Bin	1	2	3	4	5	6	7	8	9	10	11
1	1.00										
2	0.99	1.00									
3	0.99	1.00	1.00								
4	1.00	1.00	1.00	1.00							
5	1.00	0.99	0.99	1.00	1.00						
6	0.99	0.98	0.99	0.99	0.99	1.00					
7	0.99	0.98	0.99	0.99	0.99	0.99	1.00				
8	0.99	0.98	0.98	0.99	0.99	1.00	0.98	1.00			
9	0.97	0.96	0.97	0.97	0.98	0.99	0.98	0.98	1.00		
10	0.96	0.95	0.96	0.96	0.97	0.99	0.98	0.98	0.99	1.00	
11	0.94	0.95	0.96	0.95	0.95	0.96	0.95	0.95	0.95	0.97	1.00

Table 18. Correlation matrix for the efficiency uncertainty of the one-dimensional ϕ_{η}^{*} measurement.

JHEP02(2024)070

References

[1] P.J. Rijken and W.L. van Neerven, *Order α_s^2 contributions to the Drell-Yan cross-section at fixed target energies*, Phys. Rev. D **51** (1995) 44 [hep-ph/9408366] [INSPIRE].

[2] R. Hamberg, W.L. van Neerven and T. Matsuura, *A complete calculation of the order α_s^2 correction to the Drell-Yan K factor*, Nucl. Phys. B **359** (1991) 343 [INSPIRE].

[3] R.V. Harlander and W.B. Kilgore, *Next-to-next-to-leading order Higgs production at hadron colliders*, Phys. Rev. Lett. **88** (2002) 201801 [hep-ph/0201206] [INSPIRE].

[4] W.L. van Neerven and E.B. Zijlstra, *The $O(\alpha_s^2)$ corrected Drell-Yan K factor in the DIS and MS scheme*, Nucl. Phys. B **382** (1992) 11 [INSPIRE].

[5] C. Anastasiou, L.J. Dixon, K. Melnikov and F. Petriello, *High precision QCD at hadron colliders: electroweak gauge boson rapidity distributions at NNLO*, Phys. Rev. D **69** (2004) 094008 [hep-ph/0312266] [INSPIRE].

[6] I. Scimemi and A. Vladimirov, *Non-perturbative structure of semi-inclusive deep-inelastic and Drell-Yan scattering at small transverse momentum*, JHEP **06** (2020) 137 [arXiv:1912.06532] [INSPIRE].

[7] M. Bury et al., *PDF bias and flavor dependence in TMD distributions*, JHEP **10** (2022) 118 [arXiv:2201.07114] [INSPIRE].

[8] S. Camarda, L. Cieri and G. Ferrera, *Drell-Yan lepton-pair production: q_T resummation at N^3LL accuracy and fiducial cross sections at N^3LO*, Phys. Rev. D **104** (2021) L111503 [arXiv:2103.04974] [INSPIRE].

[9] C. Duhr and B. Mistlberger, *Lepton-pair production at hadron colliders at N^3LO in QCD*, JHEP **03** (2022) 116 [arXiv:2111.10379] [INSPIRE].

[10] H1 and ZEUS collaborations, *Combined measurement and QCD analysis of the inclusive $e^{\pm}p$ scattering cross sections at HERA*, JHEP **01** (2010) 109 [arXiv:0911.0884] [INSPIRE].

[11] H1 and ZEUS collaborations, *Combination of measurements of inclusive deep inelastic $e^{\pm}p$ scattering cross sections and QCD analysis of HERA data*, Eur. Phys. J. C **75** (2015) 580 [arXiv:1506.06042] [INSPIRE].

[12] CDF collaboration, *Forward-backward charge asymmetry of electron pairs above the Z^0 pole*, Phys. Rev. Lett. **77** (1996) 2616 [INSPIRE].

[13] CDF collaboration, *Measurement of the forward-backward charge asymmetry from $W \to e\nu$ production in $p\bar{p}$ collisions at $\sqrt{s} = 1.96$ TeV*, Phys. Rev. D **71** (2005) 051104 [hep-ex/0501023] [INSPIRE].

[14] CDF collaboration, *Measurement of $d\sigma/dy$ of Drell-Yan e^+e^- pairs in the Z mass region from $p\bar{p}$ collisions at $\sqrt{s} = 1.96$ TeV*, Phys. Lett. B **692** (2010) 232 [arXiv:0908.3914] [INSPIRE].

[15] CDF collaboration, *Measurement of the inclusive jet cross section at the Fermilab Tevatron $p\bar{p}$ collider using a cone-based jet algorithm*, Phys. Rev. D **78** (2008) 052006 [*Erratum ibid.* **79** (2009) 119902] [arXiv:0807.2204] [INSPIRE].

[16] D0 collaboration, *Measurement of the muon charge asymmetry from W boson decays*, Phys. Rev. D **77** (2008) 011106 [arXiv:0709.4254] [INSPIRE].

[17] D0 collaboration, *Measurement of the ratios of the $Z/\gamma^*+\geq n$ jet production cross sections to the total inclusive Z/γ^* cross section in $p\bar{p}$ collisions at $\sqrt{s}=1.96$ TeV*, Phys. Lett. B **658** (2008) 112 [hep-ex/0608052] [INSPIRE].

[18] D0 collaboration, *Measurement of the electron charge asymmetry in $p\bar{p}\to W+X\to e\nu+X$ decays in $p\bar{p}$ collisions at $\sqrt{s}=1.96$ TeV*, Phys. Rev. D **91** (2015) 032007 [*Erratum ibid.* **91** (2015) 079901] [arXiv:1412.2862] [INSPIRE].

[19] D0 collaboration, *Measurement of the inclusive jet cross-section in $p\bar{p}$ collisions at $\sqrt{s}=1.96$ TeV*, Phys. Rev. Lett. **101** (2008) 062001 [arXiv:0802.2400] [INSPIRE].

[20] ATLAS collaboration, *Measurement of the inclusive $W^\pm$ and Z/γ^* cross sections in the electron and muon decay channels in pp collisions at $\sqrt{s}=7$ TeV with the ATLAS detector*, Phys. Rev. D **85** (2012) 072004 [arXiv:1109.5141] [INSPIRE].

[21] ATLAS collaboration, *Measurement of the transverse momentum and ϕ^*_η distributions of Drell-Yan lepton pairs in proton-proton collisions at $\sqrt{s}=8$ TeV with the ATLAS detector*, Eur. Phys. J. C **76** (2016) 291 [arXiv:1512.02192] [INSPIRE].

[22] CMS collaboration, *Measurement of the muon charge asymmetry in inclusive $pp\to W+X$ production at $\sqrt{s}=7$ TeV and an improved determination of light parton distribution functions*, Phys. Rev. D **90** (2014) 032004 [arXiv:1312.6283] [INSPIRE].

[23] CMS collaboration, *Measurement of the electron charge asymmetry in inclusive W production in pp collisions at $\sqrt{s}=7$ TeV*, Phys. Rev. Lett. **109** (2012) 111806 [arXiv:1206.2598] [INSPIRE].

[24] ATLAS collaboration, *Measurement of the transverse momentum distribution of Drell-Yan lepton pairs in proton-proton collisions at $\sqrt{s}=13$ TeV with the ATLAS detector*, Eur. Phys. J. C **80** (2020) 616 [arXiv:1912.02844] [INSPIRE].

[25] CMS collaboration, *Measurements of differential Z boson production cross sections in proton-proton collisions at $\sqrt{s}=13$ TeV*, JHEP **12** (2019) 061 [arXiv:1909.04133] [INSPIRE].

[26] LHCb collaboration, *Measurement of the forward W boson cross-section in pp collisions at $\sqrt{s}=7$ TeV*, JHEP **12** (2014) 079 [arXiv:1408.4354] [INSPIRE].

[27] LHCb collaboration, *Measurement of the forward Z boson production cross-section in pp collisions at $\sqrt{s}=7$ TeV*, JHEP **08** (2015) 039 [arXiv:1505.07024] [INSPIRE].

[28] LHCb collaboration, *Measurement of forward $Z\to e^+e^-$ production at $\sqrt{s}=8$ TeV*, JHEP **05** (2015) 109 [arXiv:1503.00963] [INSPIRE].

[29] LHCb collaboration, *Measurement of forward W and Z boson production in pp collisions at $\sqrt{s}=8$ TeV*, JHEP **01** (2016) 155 [arXiv:1511.08039] [INSPIRE].

[30] LHCb collaboration, *Measurement of forward $W\to e\nu$ production in pp collisions at $\sqrt{s}=8$ TeV*, JHEP **10** (2016) 030 [arXiv:1608.01484] [INSPIRE].

[31] LHCb collaboration, *Measurement of the forward Z boson production cross-section in pp collisions at $\sqrt{s}=13$ TeV*, JHEP **09** (2016) 136 [arXiv:1607.06495] [INSPIRE].

[32] LHCb collaboration, *Precision measurement of forward Z boson production in proton-proton collisions at $\sqrt{s}=13$ TeV*, JHEP **07** (2022) 026 [arXiv:2112.07458] [INSPIRE].

[33] S. Dulat et al., *New parton distribution functions from a global analysis of quantum chromodynamics*, Phys. Rev. D **93** (2016) 033006 [arXiv:1506.07443] [INSPIRE].

[34] L.A. Harland-Lang, A.D. Martin, P. Motylinski and R.S. Thorne, *Parton distributions in the LHC era: MMHT* 2014 *PDFs*, *Eur. Phys. J. C* **75** (2015) 204 [arXiv:1412.3989] [INSPIRE].

[35] NNPDF collaboration, *Parton distributions for the LHC run II*, *JHEP* **04** (2015) 040 [arXiv:1410.8849] [INSPIRE].

[36] T.-J. Hou et al., *New CTEQ global analysis of quantum chromodynamics with high-precision data from the LHC*, *Phys. Rev. D* **103** (2021) 014013 [arXiv:1912.10053] [INSPIRE].

[37] NNPDF collaboration, *Parton distributions from high-precision collider data*, *Eur. Phys. J. C* **77** (2017) 663 [arXiv:1706.00428] [INSPIRE].

[38] NNPDF collaboration, *The path to proton structure at* 1% *accuracy*, *Eur. Phys. J. C* **82** (2022) 428 [arXiv:2109.02653] [INSPIRE].

[39] S. Bailey et al., *Parton distributions from LHC, HERA, Tevatron and fixed target data: MSHT*20 *PDFs*, *Eur. Phys. J. C* **81** (2021) 341 [arXiv:2012.04684] [INSPIRE].

[40] K.J. Eskola, H. Paukkunen and C.A. Salgado, *EPS*09*: a new generation of NLO and LO nuclear parton distribution functions*, *JHEP* **04** (2009) 065 [arXiv:0902.4154] [INSPIRE].

[41] A.D. Martin, W.J. Stirling, R.S. Thorne and G. Watt, *Parton distributions for the LHC*, *Eur. Phys. J. C* **63** (2009) 189 [arXiv:0901.0002] [INSPIRE].

[42] LHCb collaboration, *Observation of Z production in proton-lead collisions at LHCb*, *JHEP* **09** (2014) 030 [arXiv:1406.2885] [INSPIRE].

[43] LHCb collaboration, *Precision luminosity measurements at LHCb*, 2014 *JINST* **9** P12005 [arXiv:1410.0149] [INSPIRE].

[44] LHCb collaboration, *The LHCb detector at the LHC*, 2008 *JINST* **3** S08005 [INSPIRE].

[45] LHCb collaboration, *LHCb detector performance*, *Int. J. Mod. Phys. A* **30** (2015) 1530022 [arXiv:1412.6352] [INSPIRE].

[46] R. Aaij et al., *Performance of the LHCb vertex locator*, 2014 *JINST* **9** P09007 [arXiv:1405.7808] [INSPIRE].

[47] LHCb collaboration, *LHCb technical design report: reoptimized detector design and performance*, CERN-LHCC-2003-030, CERN, Geneva, Switzerland (2003) [INSPIRE].

[48] LHCb Outer Tracker Group collaboration, *Improved performance of the LHCb outer tracker in LHC run* 2, 2017 *JINST* **12** P11016 [arXiv:1708.00819] [INSPIRE].

[49] A.A. Alves Jr. et al., *Performance of the LHCb muon system*, 2013 *JINST* **8** P02022 [arXiv:1211.1346] [INSPIRE].

[50] R. Aaij et al., *The LHCb trigger and its performance in* 2011, 2013 *JINST* **8** P04022 [arXiv:1211.3055] [INSPIRE].

[51] T. Sjöstrand, S. Mrenna and P.Z. Skands, *PYTHIA* 6.4 *physics and manual*, *JHEP* **05** (2006) 026 [hep-ph/0603175] [INSPIRE].

[52] C. Bierlich et al., *A comprehensive guide to the physics and usage of PYTHIA* 8.3, *SciPost Phys. Codeb.* **2022** (2022) 8 [arXiv:2203.11601] [INSPIRE].

[53] LHCb collaboration, *Handling of the generation of primary events in Gauss, the LHCb simulation framework*, *J. Phys. Conf. Ser.* **331** (2011) 032047 [INSPIRE].

[54] N. Davidson, T. Przedzinski and Z. Was, *PHOTOS interface in C++: technical and physics documentation*, *Comput. Phys. Commun.* **199** (2016) 86 [arXiv:1011.0937] [INSPIRE].

JHEP02(2024)070

[55] J. Allison et al., *GEANT4 developments and applications*, *IEEE Trans. Nucl. Sci.* **53** (2006) 270 [INSPIRE].

[56] LHCb collaboration, *The LHCb simulation application, Gauss: design, evolution and experience*, *J. Phys. Conf. Ser.* **331** (2011) 032023 [INSPIRE].

[57] C. Balazs and C.P. Yuan, *Soft gluon effects on lepton pairs at hadron colliders*, *Phys. Rev. D* **56** (1997) 5558 [hep-ph/9704258] [INSPIRE].

[58] J.C. Collins, D.E. Soper and G.F. Sterman, *Transverse momentum distribution in Drell-Yan pair and W and Z boson production*, *Nucl. Phys. B* **250** (1985) 199 [INSPIRE].

[59] J.C. Collins and D.E. Soper, *Back-to-back jets in QCD*, *Nucl. Phys. B* **193** (1981) 381 [*Erratum ibid.* **213** (1983) 545] [INSPIRE].

[60] J.C. Collins and D.E. Soper, *Back-to-back jets: Fourier transform from B to K-transverse*, *Nucl. Phys. B* **197** (1982) 446 [INSPIRE].

[61] P. Nason, *A new method for combining NLO QCD with shower Monte Carlo algorithms*, *JHEP* **11** (2004) 040 [hep-ph/0409146] [INSPIRE].

[62] S. Frixione, P. Nason and C. Oleari, *Matching NLO QCD computations with parton shower simulations: the POWHEG method*, *JHEP* **11** (2007) 070 [arXiv:0709.2092] [INSPIRE].

[63] S. Alioli, P. Nason, C. Oleari and E. Re, *NLO vector-boson production matched with shower in POWHEG*, *JHEP* **07** (2008) 060 [arXiv:0805.4802] [INSPIRE].

[64] S. Alioli, P. Nason, C. Oleari and E. Re, *A general framework for implementing NLO calculations in shower Monte Carlo programs: the POWHEG BOX*, *JHEP* **06** (2010) 043 [arXiv:1002.2581] [INSPIRE].

[65] T. Sjöstrand, S. Mrenna and P.Z. Skands, *A brief introduction to PYTHIA* 8.1, *Comput. Phys. Commun.* **178** (2008) 852 [arXiv:0710.3820] [INSPIRE].

[66] J. Campbell and T. Neumann, *Precision phenomenology with MCFM*, *JHEP* **12** (2019) 034 [arXiv:1909.09117] [INSPIRE].

[67] A. Banfi et al., *Optimisation of variables for studying dilepton transverse momentum distributions at hadron colliders*, *Eur. Phys. J. C* **71** (2011) 1600 [arXiv:1009.1580] [INSPIRE].

[68] LHCb collaboration, *Measurement of the W boson mass*, *JHEP* **01** (2022) 036 [arXiv:2109.01113] [INSPIRE].

[69] LHCb collaboration, *Measurement of the track reconstruction efficiency at LHCb*, 2015 *JINST* **10** P02007 [arXiv:1408.1251] [INSPIRE].

[70] H.B. Prosper and L. Lyons, *Proceedings, PHYSTAT* 2011 *workshop on statistical issues related to discovery claims in search experiments and unfolding, CERN, Geneva, Switzerland* 17–20 *January* 2011, CERN, Geneva, Switzerland (2011) [DOI:10.5170/CERN-2011-006] [INSPIRE].

[71] G. D'Agostini, *A multidimensional unfolding method based on Bayes' theorem*, *Nucl. Instrum. Meth. A* **362** (1995) 487 [INSPIRE].

[72] T. Adye, *Unfolding algorithms and tests using RooUnfold*, in the proceedings of the *PHYSTAT* 2011, Geneva, Switzerland (2011), p. 313 [DOI:10.5170/CERN-2011-006.313] [arXiv:1105.1160] [INSPIRE].

[73] J. Pumplin et al., *New generation of parton distributions with uncertainties from global QCD analysis*, *JHEP* **07** (2002) 012 [hep-ph/0201195] [INSPIRE].

[74] Y. Li and F. Petriello, *Combining QCD and electroweak corrections to dilepton production in FEWZ*, *Phys. Rev. D* **86** (2012) 094034 [arXiv:1208.5967] [INSPIRE].

The LHCb collaboration

R. Aaij[32], A.S.W. Abdelmotteleb[51], C. Abellan Beteta[45], F. Abudinén[51], T. Ackernley[55], B. Adeva[41], M. Adinolfi[49], P. Adlarson[77], H. Afsharnia[9], C. Agapopoulou[43], C.A. Aidala[78], Z. Ajaltouni[9], S. Akar[60], K. Akiba[32], P. Albicocco[23], J. Albrecht[15], F. Alessio[43], M. Alexander[54], A. Alfonso Albero[40], Z. Aliouche[57], P. Alvarez Cartelle[50], R. Amalric[13], S. Amato[2], J.L. Amey[49], Y. Amhis[11,43], L. An[5], L. Anderlini[22], M. Andersson[45], A. Andreianov[38], P. Andreola[45], M. Andreotti[21], D. Andreou[63], D. Ao[6], F. Archilli[31,u], A. Artamonov[38], M. Artuso[63], E. Aslanides[10], M. Atzeni[59], B. Audurier[12], I. Bachiller Perea[8], S. Bachmann[17], M. Bachmayer[44], J.J. Back[51], A. Bailly-reyre[13], P. Baladron Rodriguez[41], V. Balagura[12], W. Baldini[21,43], J. Baptista de Souza Leite[1], M. Barbetti[22,l], I. R. Barbosa[65], R.J. Barlow[57], S. Barsuk[11], W. Barter[53], M. Bartolini[50], F. Baryshnikov[38], J.M. Basels[14], G. Bassi[29,r], B. Batsukh[4], A. Battig[15], A. Bay[44], A. Beck[51], M. Becker[15], F. Bedeschi[29], I.B. Bediaga[1], A. Beiter[63], S. Belin[41], V. Bellee[45], K. Belous[38], I. Belov[24], I. Belyaev[38], G. Benane[10], G. Bencivenni[23], E. Ben-Haim[13], A. Berezhnoy[38], R. Bernet[45], S. Bernet Andres[39], D. Berninghoff[17], H.C. Bernstein[63], C. Bertella[57], A. Bertolin[28], C. Betancourt[45], F. Betti[53], J. Bex[50], Ia. Bezshyiko[45], J. Bhom[35], L. Bian[69], M.S. Bieker[15], N.V. Biesuz[21], P. Billoir[13], A. Biolchini[32], M. Birch[56], F.C.R. Bishop[50], A. Bitadze[57], A. Bizzeti, M.P. Blago[50], T. Blake[51], F. Blanc[44], J.E. Blank[15], S. Blusk[63], D. Bobulska[54], V. Bocharnikov[38], J.A. Boelhauve[15], O. Boente Garcia[12], T. Boettcher[60], A. Bohare[53], A. Boldyrev[38], C.S. Bolognani[75], R. Bolzonella[21,k], N. Bondar[38], F. Borgato[28,43], S. Borghi[57], M. Borsato[17], J.T. Borsuk[35], S.A. Bouchiba[44], T.J.V. Bowcock[55], A. Boyer[43], C. Bozzi[21], M.J. Bradley[56], S. Braun[61], A. Brea Rodriguez[41], N. Breer[15], J. Brodzicka[35], A. Brossa Gonzalo[41], J. Brown[55], D. Brundu[27], A. Buonaura[45], L. Buonincontri[28], A.T. Burke[57], C. Burr[43], A. Bursche[67], A. Butkevich[38], J.S. Butter[32], J. Buytaert[43], W. Byczynski[43], S. Cadeddu[27], H. Cai[69], R. Calabrese[21,k], L. Calefice[15], S. Cali[23], M. Calvi[26,o], M. Calvo Gomez[39], J. Cambon Bouzas[41], P. Campana[23], D.H. Campora Perez[75], A.F. Campoverde Quezada[6], S. Capelli[26,o], L. Capriotti[21], A. Carbone[20,i], L. Carcedo Salgado[41], R. Cardinale[24,m], A. Cardini[27], P. Carniti[26,o], L. Carus[17], A. Casais Vidal[41], R. Caspary[17], G. Casse[55], M. Cattaneo[43], G. Cavallero[21], V. Cavallini[21,k], S. Celani[44], J. Cerasoli[10], D. Cervenkov[58], A.J. Chadwick[55], I. Chahrour[78], M.G. Chapman[49], M. Charles[13], Ph. Charpentier[43], C.A. Chavez Barajas[55], M. Chefdeville[8], C. Chen[10], S. Chen[4], A. Chernov[35], S. Chernyshenko[47], V. Chobanova[41,x], S. Cholak[44], M. Chrzaszcz[35], A. Chubykin[38], V. Chulikov[38], P. Ciambrone[23], M.F. Cicala[51], X. Cid Vidal[41], G. Ciezarek[43], P. Cifra[43], P.E.L. Clarke[53], M. Clemencic[43], H.V. Cliff[50], J. Closier[43], J.L. Cobbledick[57], C. Cocha Toapaxi[17], V. Coco[43], J. Cogan[10], E. Cogneras[9], L. Cojocariu[37], P. Collins[43], T. Colombo[43], A. Comerma-Montells[40], L. Congedo[19], A. Contu[27], N. Cooke[54], I. Corredoira [41], A. Correia[13], G. Corti[43], J.J. Cottee Meldrum[49], B. Couturier[43], D.C. Craik[45], M. Cruz Torres[1,g], R. Currie[53], C.L. Da Silva[62], S. Dadabaev[38], L. Dai[66], X. Dai[5], E. Dall'Occo[15], J. Dalseno[41], C. D'Ambrosio[43], J. Daniel[9], A. Danilina[38], P. d'Argent[19], A. Davidson[51], J.E. Davies[57], A. Davis[57], O. De Aguiar Francisco[57], J. de Boer[32], K. De Bruyn[74], S. De Capua[57], M. De Cian[17],

JHEP02(2024)070

U. De Freitas Carneiro Da Graca[1], E. De Lucia[23], J.M. De Miranda[1], L. De Paula[2], M. De Serio[19,h], D. De Simone[45], P. De Simone[23], F. De Vellis[15], J.A. de Vries[75], C.T. Dean[62], F. Debernardis[19,h], D. Decamp[8], V. Dedu[10], L. Del Buono[13], B. Delaney[59], H.-P. Dembinski[15], V. Denysenko[45], O. Deschamps[9], F. Dettori[27,j], B. Dey[72], P. Di Nezza[23], I. Diachkov[38], S. Didenko[38], S. Ding[63], V. Dobishuk[47], A. D. Docheva[54], A. Dolmatov[38], C. Dong[3], A.M. Donohoe[18], F. Dordei[27], A.C. dos Reis[1], L. Douglas[54], A.G. Downes[8], W. Duan[67], P. Duda[76], M.W. Dudek[35], L. Dufour[43], V. Duk[73], P. Durante[43], M. M. Duras[76], J.M. Durham[62], D. Dutta[57], A. Dziurda[35], A. Dzyuba[38], S. Easo[52,43], E. Eckstein[71], U. Egede[64], A. Egorychev[38], V. Egorychev[38], C. Eirea Orro[41], S. Eisenhardt[53], E. Ejopu[57], S. Ek-In[44], L. Eklund[77], M. Elashri[60], J. Ellbracht[15], S. Ely[56], A. Ene[37], E. Epple[60], S. Escher[14], J. Eschle[45], S. Esen[45], T. Evans[57], F. Fabiano[27,j,43], L.N. Falcao[1], Y. Fan[6], B. Fang[69,11], L. Fantini[73,q], M. Faria[44], K. Farmer[53], S. Farry[55], D. Fazzini[26,o], L. Felkowski[76], M. Feng[4,6], M. Feo[43], M. Fernandez Gomez[41], A.D. Fernez[61], F. Ferrari[20], L. Ferreira Lopes[44], F. Ferreira Rodrigues[2], S. Ferreres Sole[32], M. Ferrillo[45], M. Ferro-Luzzi[43], S. Filippov[38], R.A. Fini[19], M. Fiorini[21,k], M. Firlej[34], K.M. Fischer[58], D.S. Fitzgerald[78], C. Fitzpatrick[57], T. Fiutowski[34], F. Fleuret[12], M. Fontana[20], F. Fontanelli[24,m], L. F. Foreman[57], R. Forty[43], D. Foulds-Holt[50], M. Franco Sevilla[61], M. Frank[43], E. Franzoso[21,k], G. Frau[17], C. Frei[43], D.A. Friday[57], L. Frontini[25,n], J. Fu[6], Q. Fuehring[15], Y. Fujii[64], T. Fulghesu[13], E. Gabriel[32], G. Galati[19,h], M.D. Galati[32], A. Gallas Torreira[41], D. Galli[20,i], S. Gambetta[53,43], M. Gandelman[2], P. Gandini[25], H. Gao[6], R. Gao[58], Y. Gao[7], Y. Gao[5], M. Garau[27,j], L.M. Garcia Martin[44], P. Garcia Moreno[40], J. García Pardiñas[43], B. Garcia Plana[41], F.A. Garcia Rosales[12], L. Garrido[40], C. Gaspar[43], R.E. Geertsema[32], L.L. Gerken[15], E. Gersabeck[57], M. Gersabeck[57], T. Gershon[51], L. Giambastiani[28], F. I. Giasemis[13,e], V. Gibson[50], H.K. Giemza[36], A.L. Gilman[58], M. Giovannetti[23], A. Gioventù[41], P. Gironella Gironell[40], C. Giugliano[21,k], M.A. Giza[35], K. Gizdov[53], E.L. Gkougkousis[43], F.C. Glaser[11,17], V.V. Gligorov[13], C. Göbel[65], E. Golobardes[39], D. Golubkov[38], A. Golutvin[56,38,43], A. Gomes[1,2,b,a,†], S. Gomez Fernandez[40], F. Goncalves Abrantes[58], M. Goncerz[35], G. Gong[3], J. A. Gooding[15], I.V. Gorelov[38], C. Gotti[26], J.P. Grabowski[71], L.A. Granado Cardoso[43], E. Graugés[40], E. Graverini[44], G. Graziani, A. T. Grecu[37], L.M. Greeven[32], N.A. Grieser[60], L. Grillo[54], S. Gromov[38], C. Gu[12], M. Guarise[21], M. Guittiere[11], V. Guliaeva[38], P. A. Günther[17], A.-K. Guseinov[38], E. Gushchin[38], Y. Guz[5,38,43], T. Gys[43], T. Hadavizadeh[64], C. Hadjivasiliou[61], G. Haefeli[44], C. Haen[43], J. Haimberger[43], S.C. Haines[50], M. Hajheidari[43], T. Halewood-leagas[55], M.M. Halvorsen[43], P.M. Hamilton[61], J. Hammerich[55], Q. Han[7], X. Han[17], S. Hansmann-Menzemer[17], L. Hao[6], N. Harnew[58], T. Harrison[55], M. Hartmann[11], C. Hasse[43], M. Hatch[43], J. He[6,d], K. Heijhoff[32], F. Hemmer[43], C. Henderson[60], R.D.L. Henderson[64,51], A.M. Hennequin[43], K. Hennessy[55], L. Henry[44], J. Herd[56], J. Heuel[14], A. Hicheur[2], D. Hill[44], M. Hilton[57], S.E. Hollitt[15], J. Horswill[57], R. Hou[7], Y. Hou[8], N. Howarth[55], J. Hu[17], J. Hu[67], W. Hu[5], X. Hu[3], W. Huang[6], X. Huang[69], W. Hulsbergen[32], R.J. Hunter[51], M. Hushchyn[38], D. Hutchcroft[55], P. Ibis[15], M. Idzik[34], D. Ilin[38], P. Ilten[60], A. Inglessi[38], A. Iniukhin[38], A. Ishteev[38], K. Ivshin[38], R. Jacobsson[43],

JHEP02(2024)070

H. Jage[14], S.J. Jaimes Elles[42,70], S. Jakobsen[43], E. Jans[32], B.K. Jashal[42], A. Jawahery[61], V. Jevtic[15], E. Jiang[61], X. Jiang[4,6], Y. Jiang[6], Y. J. Jiang[5], M. John[58], D. Johnson[48], C.R. Jones[50], T.P. Jones[51], S. Joshi[36], B. Jost[43], N. Jurik[43], I. Juszczak[35], D. Kaminaris[44], S. Kandybei[46], Y. Kang[3], M. Karacson[43], D. Karpenkov[38], M. Karpov[38], A. M. Kauniskangas[44], J.W. Kautz[60], F. Keizer[43], D.M. Keller[63], M. Kenzie[51], T. Ketel[32], B. Khanji[63], A. Kharisova[38], S. Kholodenko[38], G. Khreich[11], T. Kirn[14], V.S. Kirsebom[44], O. Kitouni[59], S. Klaver[33], N. Kleijne[29,r], K. Klimaszewski[36], M.R. Kmiec[36], S. Koliiev[47], L. Kolk[15], A. Kondybayeva[38], A. Konoplyannikov[38], P. Kopciewicz[34,43], R. Kopecna[17], P. Koppenburg[32], M. Korolev[38], I. Kostiuk[32], O. Kot[47], S. Kotriakhova, A. Kozachuk[38], P. Kravchenko[38], L. Kravchuk[38], M. Kreps[51], S. Kretzschmar[14], P. Krokovny[38], W. Krupa[63], W. Krzemien[36], J. Kubat[17], S. Kubis[76], W. Kucewicz[35], M. Kucharczyk[35], V. Kudryavtsev[38], E. Kulikova[38], A. Kupsc[77], B. K. Kutsenko[10], D. Lacarrere[43], G. Lafferty[57], A. Lai[27], A. Lampis[27,j], D. Lancierini[45], C. Landesa Gomez[41], J.J. Lane[64], R. Lane[49], C. Langenbruch[17], J. Langer[15], O. Lantwin[38], T. Latham[51], F. Lazzari[29,s], C. Lazzeroni[48], R. Le Gac[10], S.H. Lee[78], R. Lefèvre[9], A. Leflat[38], S. Legotin[38], O. Leroy[10], T. Lesiak[35], B. Leverington[17], A. Li[3], H. Li[67], K. Li[7], L. Li[57], P. Li[43], P.-R. Li[68], S. Li[7], T. Li[4], T. Li[67], Y. Li[4], Z. Li[63], Z. Lian[3], X. Liang[63], C. Lin[6], T. Lin[52], R. Lindner[43], V. Lisovskyi[44], R. Litvinov[27,j], G. Liu[67], H. Liu[6], K. Liu[68], Q. Liu[6], S. Liu[4,6], Y. Liu[68], A. Lobo Salvia[40], A. Loi[27], J. Lomba Castro[41], T. Long[50], I. Longstaff[54], J.H. Lopes[2], A. Lopez Huertas[40], S. López Soliño[41], G.H. Lovell[50], Y. Lu[4,c], C. Lucarelli[22,l], D. Lucchesi[28,p], S. Luchuk[38], M. Lucio Martinez[75], V. Lukashenko[32,47], Y. Luo[3], A. Lupato[28], E. Luppi[21,k], K. Lynch[18], X.-R. Lyu[6], R. Ma[6], S. Maccolini[15], F. Machefert[11], F. Maciuc[37], I. Mackay[58], V. Macko[44], L.R. Madhan Mohan[50], M. M. Madurai[48], A. Maevskiy[38], D. Maisuzenko[38], M.W. Majewski[34], J.J. Malczewski[35], S. Malde[58], B. Malecki[35,43], A. Malinin[38], T. Maltsev[38], G. Manca[27,j], G. Mancinelli[10], C. Mancuso[25,11,n], R. Manera Escalero[40], D. Manuzzi[20], C.A. Manzari[45], D. Marangotto[25,n], J.F. Marchand[8], U. Marconi[20], S. Mariani[43], C. Marin Benito[40], J. Marks[17], A.M. Marshall[49], P.J. Marshall[55], G. Martelli[73,q], G. Martellotti[30], L. Martinazzoli[43,o], M. Martinelli[26,o], D. Martinez Santos[41], F. Martinez Vidal[42], A. Massafferri[1], M. Materok[14], R. Matev[43], A. Mathad[45], V. Matiunin[38], C. Matteuzzi[63,26], K.R. Mattioli[12], A. Mauri[56], E. Maurice[12], J. Mauricio[40], M. Mazurek[43], M. McCann[56], L. Mcconnell[18], T.H. McGrath[57], N.T. McHugh[54], A. McNab[57], R. McNulty[18], B. Meadows[60], G. Meier[15], D. Melnychuk[36], M. Merk[32,75], A. Merli[25,n], L. Meyer Garcia[2], D. Miao[4,6], H. Miao[6], M. Mikhasenko[71,f], D.A. Milanes[70], M. Milovanovic[43], M.-N. Minard[8,†], A. Minotti[26,o], E. Minucci[63], T. Miralles[9], S.E. Mitchell[53], B. Mitreska[15], D.S. Mitzel[15], A. Modak[52], A. Mödden [15], R.A. Mohammed[58], R.D. Moise[14], S. Mokhnenko[38], T. Mombächer[41], M. Monk[51,64], I.A. Monroy[70], S. Monteil[9], G. Morello[23], M.J. Morello[29,r], M.P. Morgenthaler[17], J. Moron[34], A.B. Morris[43], A.G. Morris[10], R. Mountain[63], H. Mu[3], Z. M. Mu[5], E. Muhammad[51], F. Muheim[53], M. Mulder[74], K. Müller[45], D. Murray[57], R. Murta[56], P. Naik[55], T. Nakada[44], R. Nandakumar[52], T. Nanut[43], I. Nasteva[2], M. Needham[53], N. Neri[25,n], S. Neubert[71], N. Neufeld[43], P. Neustroev[38], R. Newcombe[56], J. Nicolini[15,11],

D. Nicotra[75], E.M. Niel[44], S. Nieswand[14], N. Nikitin[38], P. Nogga[71], N.S. Nolte[59], C. Normand[8,j,27], J. Novoa Fernandez[41], G. Nowak[60], C. Nunez[78], H. N. Nur[54], A. Oblakowska-Mucha[34], V. Obraztsov[38], T. Oeser[14], S. Okamura[21,k,43], R. Oldeman[27,j], F. Oliva[53], M. Olocco[15], C.J.G. Onderwater[75], R.H. O'Neil[53], J.M. Otalora Goicochea[2], T. Ovsiannikova[38], P. Owen[45], A. Oyanguren[42], O. Ozcelik[53], K.O. Padeken[71], B. Pagare[51], P.R. Pais[17], T. Pajero[58], A. Palano[19], M. Palutan[23], G. Panshin[38], L. Paolucci[51], A. Papanestis[52], M. Pappagallo[19,h], L.L. Pappalardo[21,k], C. Pappenheimer[60], C. Parkes[57,43], B. Passalacqua[21,k], G. Passaleva[22], A. Pastore[19], M. Patel[56], J. Patoc[58], C. Patrignani[20,i], C.J. Pawley[75], A. Pellegrino[32], M. Pepe Altarelli[23], S. Perazzini[20], D. Pereima[38], A. Pereiro Castro[41], P. Perret[9], A. Perro[43], K. Petridis[49], A. Petrolini[24,m], S. Petrucci[53], H. Pham[63], A. Philippov[38], L. Pica[29,r], M. Piccini[73], B. Pietrzyk[8], G. Pietrzyk[11], D. Pinci[30], F. Pisani[43], M. Pizzichemi[26,o], V. Placinta[37], M. Plo Casasus[41], F. Polci[13,43], M. Poli Lener[23], A. Poluektov[10], N. Polukhina[38], I. Polyakov[43], E. Polycarpo[2], S. Ponce[43], D. Popov[6], S. Poslavskii[38], K. Prasanth[35], L. Promberger[17], C. Prouve[41], V. Pugatch[47], V. Puill[11], G. Punzi[29,s], H.R. Qi[3], W. Qian[6], N. Qin[3], S. Qu[3], R. Quagliani[44], B. Rachwal[34], J.H. Rademacker[49], R. Rajagopalan[63], M. Rama[29], M. Ramírez García[78], M. Ramos Pernas[51], M.S. Rangel[2], F. Ratnikov[38], G. Raven[33], M. Rebollo De Miguel[42], F. Redi[43], J. Reich[49], F. Reiss[57], Z. Ren[3], P.K. Resmi[58], R. Ribatti[29,r], G. R. Ricart[12,79], S. Ricciardi[52], K. Richardson[59], M. Richardson-Slipper[53], K. Rinnert[55], P. Robbe[11], G. Robertson[53], E. Rodrigues[55,43], E. Rodriguez Fernandez[41], J.A. Rodriguez Lopez[70], E. Rodriguez Rodriguez[41], D.L. Rolf[43], A. Rollings[58], P. Roloff[43], V. Romanovskiy[38], M. Romero Lamas[41], A. Romero Vidal[41], F. Ronchetti[44], M. Rotondo[23], M.S. Rudolph[63], T. Ruf[43], R.A. Ruiz Fernandez[41], J. Ruiz Vidal[42], A. Ryzhikov[38], J. Ryzka[34], J.J. Saborido Silva[41], N. Sagidova[38], N. Sahoo[48], B. Saitta[27,j], M. Salomoni[43], C. Sanchez Gras[32], I. Sanderswood[42], R. Santacesaria[30], C. Santamarina Rios[41], M. Santimaria[23], L. Santoro [1], E. Santovetti[31], D. Saranin[38], G. Sarpis[53], M. Sarpis[71], A. Sarti[30], C. Satriano[30,t], A. Satta[31], M. Saur[5], D. Savrina[38], H. Sazak[9], L.G. Scantlebury Smead[58], A. Scarabotto[13], S. Schael[14], S. Scherl[55], A. M. Schertz[72], M. Schiller[54], H. Schindler[43], M. Schmelling[16], B. Schmidt[43], S. Schmitt[14], O. Schneider[44], A. Schopper[43], M. Schubiger[32], N. Schulte[15], S. Schulte[44], M.H. Schune[11], R. Schwemmer[43], G. Schwering[14], B. Sciascia[23], A. Sciuccati[43], S. Sellam[41], A. Semennikov[38], M. Senghi Soares[33], A. Sergi[24,m], N. Serra[45,43], L. Sestini[28], A. Seuthe[15], Y. Shang[5], D.M. Shangase[78], M. Shapkin[38], I. Shchemerov[38], L. Shchutska[44], T. Shears[55], L. Shekhtman[38], Z. Shen[5], S. Sheng[4,6], V. Shevchenko[38], B. Shi[6], E.B. Shields[26,o], Y. Shimizu[11], E. Shmanin[38], R. Shorkin[38], J.D. Shupperd[63], B.G. Siddi[21,k], R. Silva Coutinho[63], G. Simi[28], S. Simone[19,h], M. Singla[64], N. Skidmore[57], R. Skuza[17], T. Skwarnicki[63], M.W. Slater[48], J.C. Smallwood[58], J.G. Smeaton[50], E. Smith[59], K. Smith[62], M. Smith[56], A. Snoch[32], L. Soares Lavra[53], M.D. Sokoloff[60], F.J.P. Soler[54], A. Solomin[38,49], A. Solovev[38], I. Solovyev[38], R. Song[64], Y. Song[44], Y. Song[3], Y. S. Song[5], F.L. Souza De Almeida[2], B. Souza De Paula[2], E. Spadaro Norella[25,n], E. Spedicato[20], J.G. Speer[15], E. Spiridenkov[38], P. Spradlin[54], V. Sriskaran[43], F. Stagni[43], M. Stahl[43], S. Stahl[43], S. Stanislaus[58],

JHEP02(2024)070

E.N. Stein[43], O. Steinkamp[45], O. Stenyakin[38], H. Stevens[15], D. Strekalina[38], Y. Su[6], F. Suljik[58], J. Sun[27], L. Sun[69], Y. Sun[61], P.N. Swallow[48], K. Swientek[34], F. Swystun[51], A. Szabelski[36], T. Szumlak[34], M. Szymanski[43], Y. Tan[3], S. Taneja[57], M.D. Tat[58], A. Terentev[45], F. Teubert[43], E. Thomas[43], D.J.D. Thompson[48], H. Tilquin[56], V. Tisserand[9], S. T'Jampens[8], M. Tobin[4], L. Tomassetti[21,k], G. Tonani[25,n], X. Tong[5], D. Torres Machado[1], L. Toscano[15], D.Y. Tou[3], C. Trippl[44], G. Tuci[17], N. Tuning[32], A. Ukleja[36], D.J. Unverzagt[17], E. Ursov[38], A. Usachov[33], A. Ustyuzhanin[38], U. Uwer[17], V. Vagnoni[20], A. Valassi[43], G. Valenti[20], N. Valls Canudas[39], M. Van Dijk[44], H. Van Hecke[62], E. van Herwijnen[56], C.B. Van Hulse[41,w], R. Van Laak[44], M. van Veghel[32], R. Vazquez Gomez[40], P. Vazquez Regueiro[41], C. Vázquez Sierra[41], S. Vecchi[21], J.J. Velthuis[49], M. Veltri[22,v], A. Venkateswaran[44], M. Vesterinen[51], D. Vieira[60], M. Vieites Diaz[43], X. Vilasis-Cardona[39], E. Vilella Figueras[55], A. Villa[20], P. Vincent[13], F.C. Volle[11], D. vom Bruch[10], V. Vorobyev[38], N. Voropaev[38], K. Vos[75], C. Vrahas[53], J. Walsh[29], E.J. Walton[64], G. Wan[5], C. Wang[17], G. Wang[7], J. Wang[5], J. Wang[4], J. Wang[3], J. Wang[69], M. Wang[25], N. W. Wang[6], R. Wang[49], X. Wang[67], Y. Wang[7], Y. Wang[7], Z. Wang[45], Z. Wang[3], Z. Wang[6], J.A. Ward[51,64], N.K. Watson[48], D. Websdale[56], Y. Wei[5], B.D.C. Westhenry[49], D.J. White[57], M. Whitehead[54], A.R. Wiederhold[51], D. Wiedner[15], G. Wilkinson[58], M.K. Wilkinson[60], I. Williams[50], M. Williams[59], M.R.J. Williams[53], R. Williams[50], F.F. Wilson[52], W. Wislicki[36], M. Witek[35], L. Witola[17], C.P. Wong[62], G. Wormser[11], S.A. Wotton[50], H. Wu[63], J. Wu[7], Y. Wu[5], K. Wyllie[43], S. Xian[67], Z. Xiang[4], Y. Xie[7], A. Xu[29], J. Xu[6], L. Xu[3], L. Xu[3], M. Xu[51], Z. Xu[9], Z. Xu[6], Z. Xu[4], D. Yang[3], S. Yang[6], X. Yang[5], Y. Yang[24], Z. Yang[5], Z. Yang[61], V. Yeroshenko[11], H. Yeung[57], H. Yin[7], C. Y. Yu[5], J. Yu[66], X. Yuan[4], E. Zaffaroni[44], M. Zavertyaev[16], M. Zdybal[35], M. Zeng[3], C. Zhang[5], D. Zhang[7], J. Zhang[6], L. Zhang[3], S. Zhang[66], S. Zhang[5], Y. Zhang[5], Y. Zhang[58], Y. Zhao[17], A. Zharkova[38], A. Zhelezov[17], Y. Zheng[6], T. Zhou[5], X. Zhou[7], Y. Zhou[6], V. Zhovkovska[11], L. Z. Zhu[6], X. Zhu[3], X. Zhu[7], Z. Zhu[6], V. Zhukov[14,38], J. Zhuo[42], Q. Zou[4,6], S. Zucchelli[20,i], D. Zuliani[28], G. Zunica[57]

[1] *Centro Brasileiro de Pesquisas Físicas (CBPF), Rio de Janeiro, Brazil*
[2] *Universidade Federal do Rio de Janeiro (UFRJ), Rio de Janeiro, Brazil*
[3] *Center for High Energy Physics, Tsinghua University, Beijing, China*
[4] *Institute Of High Energy Physics (IHEP), Beijing, China*
[5] *School of Physics State Key Laboratory of Nuclear Physics and Technology, Peking University, Beijing, China*
[6] *University of Chinese Academy of Sciences, Beijing, China*
[7] *Institute of Particle Physics, Central China Normal University, Wuhan, Hubei, China*
[8] *Université Savoie Mont Blanc, CNRS, IN2P3-LAPP, Annecy, France*
[9] *Université Clermont Auvergne, CNRS/IN2P3, LPC, Clermont-Ferrand, France*
[10] *Aix Marseille Univ, CNRS/IN2P3, CPPM, Marseille, France*
[11] *Université Paris-Saclay, CNRS/IN2P3, IJCLab, Orsay, France*
[12] *Laboratoire Leprince-Ringuet, CNRS/IN2P3, Ecole Polytechnique, Institut Polytechnique de Paris, Palaiseau, France*
[13] *LPNHE, Sorbonne Université, Paris Diderot Sorbonne Paris Cité, CNRS/IN2P3, Paris, France*
[14] *I. Physikalisches Institut, RWTH Aachen University, Aachen, Germany*
[15] *Fakultät Physik, Technische Universität Dortmund, Dortmund, Germany*
[16] *Max-Planck-Institut für Kernphysik (MPIK), Heidelberg, Germany*

JHEP02(2024)070

[17] *Physikalisches Institut, Ruprecht-Karls-Universität Heidelberg, Heidelberg, Germany*
[18] *School of Physics, University College Dublin, Dublin, Ireland*
[19] *INFN Sezione di Bari, Bari, Italy*
[20] *INFN Sezione di Bologna, Bologna, Italy*
[21] *INFN Sezione di Ferrara, Ferrara, Italy*
[22] *INFN Sezione di Firenze, Firenze, Italy*
[23] *INFN Laboratori Nazionali di Frascati, Frascati, Italy*
[24] *INFN Sezione di Genova, Genova, Italy*
[25] *INFN Sezione di Milano, Milano, Italy*
[26] *INFN Sezione di Milano-Bicocca, Milano, Italy*
[27] *INFN Sezione di Cagliari, Monserrato, Italy*
[28] *Università degli Studi di Padova, Università e INFN, Padova, Padova, Italy*
[29] *INFN Sezione di Pisa, Pisa, Italy*
[30] *INFN Sezione di Roma La Sapienza, Roma, Italy*
[31] *INFN Sezione di Roma Tor Vergata, Roma, Italy*
[32] *Nikhef National Institute for Subatomic Physics, Amsterdam, Netherlands*
[33] *Nikhef National Institute for Subatomic Physics and VU University Amsterdam, Amsterdam, Netherlands*
[34] *AGH - University of Science and Technology, Faculty of Physics and Applied Computer Science, Kraków, Poland*
[35] *Henryk Niewodniczanski Institute of Nuclear Physics Polish Academy of Sciences, Kraków, Poland*
[36] *National Center for Nuclear Research (NCBJ), Warsaw, Poland*
[37] *Horia Hulubei National Institute of Physics and Nuclear Engineering, Bucharest-Magurele, Romania*
[38] *Affiliated with an institute covered by a cooperation agreement with CERN*
[39] *DS4DS, La Salle, Universitat Ramon Llull, Barcelona, Spain*
[40] *ICCUB, Universitat de Barcelona, Barcelona, Spain*
[41] *Instituto Galego de Física de Altas Enerxías (IGFAE), Universidade de Santiago de Compostela, Santiago de Compostela, Spain*
[42] *Instituto de Fisica Corpuscular, Centro Mixto Universidad de Valencia - CSIC, Valencia, Spain*
[43] *European Organization for Nuclear Research (CERN), Geneva, Switzerland*
[44] *Institute of Physics, Ecole Polytechnique Fédérale de Lausanne (EPFL), Lausanne, Switzerland*
[45] *Physik-Institut, Universität Zürich, Zürich, Switzerland*
[46] *NSC Kharkiv Institute of Physics and Technology (NSC KIPT), Kharkiv, Ukraine*
[47] *Institute for Nuclear Research of the National Academy of Sciences (KINR), Kyiv, Ukraine*
[48] *University of Birmingham, Birmingham, United Kingdom*
[49] *H.H. Wills Physics Laboratory, University of Bristol, Bristol, United Kingdom*
[50] *Cavendish Laboratory, University of Cambridge, Cambridge, United Kingdom*
[51] *Department of Physics, University of Warwick, Coventry, United Kingdom*
[52] *STFC Rutherford Appleton Laboratory, Didcot, United Kingdom*
[53] *School of Physics and Astronomy, University of Edinburgh, Edinburgh, United Kingdom*
[54] *School of Physics and Astronomy, University of Glasgow, Glasgow, United Kingdom*
[55] *Oliver Lodge Laboratory, University of Liverpool, Liverpool, United Kingdom*
[56] *Imperial College London, London, United Kingdom*
[57] *Department of Physics and Astronomy, University of Manchester, Manchester, United Kingdom*
[58] *Department of Physics, University of Oxford, Oxford, United Kingdom*
[59] *Massachusetts Institute of Technology, Cambridge, MA, United States*
[60] *University of Cincinnati, Cincinnati, OH, United States*
[61] *University of Maryland, College Park, MD, United States*
[62] *Los Alamos National Laboratory (LANL), Los Alamos, NM, United States*
[63] *Syracuse University, Syracuse, NY, United States*
[64] *School of Physics and Astronomy, Monash University, Melbourne, Australia, associated to* [51]
[65] *Pontifícia Universidade Católica do Rio de Janeiro (PUC-Rio), Rio de Janeiro, Brazil, associated to* [2]
[66] *Physics and Micro Electronic College, Hunan University, Changsha City, China, associated to* [7]

JHEP02(2024)070

[67] Guangdong Provincial Key Laboratory of Nuclear Science, Guangdong-Hong Kong Joint Laboratory of Quantum Matter, Institute of Quantum Matter, South China Normal University, Guangzhou, China, associated to [3]
[68] Lanzhou University, Lanzhou, China, associated to [4]
[69] School of Physics and Technology, Wuhan University, Wuhan, China, associated to [3]
[70] Departamento de Fisica , Universidad Nacional de Colombia, Bogota, Colombia, associated to [13]
[71] Universität Bonn - Helmholtz-Institut für Strahlen und Kernphysik, Bonn, Germany, associated to [17]
[72] Eotvos Lorand University, Budapest, Hungary, associated to [43]
[73] INFN Sezione di Perugia, Perugia, Italy, associated to [21]
[74] Van Swinderen Institute, University of Groningen, Groningen, Netherlands, associated to [32]
[75] Universiteit Maastricht, Maastricht, Netherlands, associated to [32]
[76] Tadeusz Kosciuszko Cracow University of Technology, Cracow, Poland, associated to [35]
[77] Department of Physics and Astronomy, Uppsala University, Uppsala, Sweden, associated to [54]
[78] University of Michigan, Ann Arbor, MI, United States, associated to [63]
[79] Departement de Physique Nucleaire (SPhN), Gif-Sur-Yvette, France

[a] Universidade de Brasília, Brasília, Brazil
[b] Universidade Federal do Triângulo Mineiro (UFTM), Uberaba-MG, Brazil
[c] Central South U., Changsha, China
[d] Hangzhou Institute for Advanced Study, UCAS, Hangzhou, China
[e] LIP6, Sorbonne Universite, Paris, France
[f] Excellence Cluster ORIGINS, Munich, Germany
[g] Universidad Nacional Autónoma de Honduras, Tegucigalpa, Honduras
[h] Università di Bari, Bari, Italy
[i] Università di Bologna, Bologna, Italy
[j] Università di Cagliari, Cagliari, Italy
[k] Università di Ferrara, Ferrara, Italy
[l] Università di Firenze, Firenze, Italy
[m] Università di Genova, Genova, Italy
[n] Università degli Studi di Milano, Milano, Italy
[o] Università di Milano Bicocca, Milano, Italy
[p] Università di Padova, Padova, Italy
[q] Università di Perugia, Perugia, Italy
[r] Scuola Normale Superiore, Pisa, Italy
[s] Università di Pisa, Pisa, Italy
[t] Università della Basilicata, Potenza, Italy
[u] Università di Roma Tor Vergata, Roma, Italy
[v] Università di Urbino, Urbino, Italy
[w] Universidad de Alcalá, Alcalá de Henares , Spain
[x] Universidade da Coruña, Coruña, Spain
[†] Deceased

JHEP02(2024)070